Gas-Phase Pyrolysis Products Emitted by Prescribed Fires in Pine Forests with a Shrub Understory in the Southeastern United States**

Nicole K. Scharko[1], Ashley M. Oeck[1], Tanya L. Myers[1], Russell G. Tonkyn[1],
Catherine A. Banach[1], Stephen P. Baker[2], Emily N. Lincoln[2], Joey Chong[3],
Bonni M. Corcoran[3], Gloria M. Burke[3], Roger D. Ottmar[4], Joseph C. Restaino[5],
David R. Weise[3], and Timothy J. Johnson[1*]

[1]Pacific Northwest National Laboratories, Richland, WA, USA
[2]USDA Forest Service, Rocky Mountain Research Station, Missoula, MT, USA
[3]USDA Forest Service, Pacific Southwest Research Station, Riverside, CA, USA
[4]USDA Forest Service, Pacific Northwest Research Station, Seattle WA, USA
[5]School of Environmental and Forest Sciences, University of Washington, Seattle WA, USA

*To whom correspondence should be addressed: Timothy.Johnson@pnnl.gov

ABSTRACT

In this study we identify pyrolysis gases from prescribed burns conducted in pine forests with a

shrub understory captured using a manual extraction device. The device selectively sampled

emissions ahead of the flame front, minimizing collection of oxidized gases, with the captured

gases analyzed in the laboratory using infrared (IR) absorption spectroscopy. Results show that

emission ratios (ER) relative to CO for ethene and acetylene were significantly greater than

previous fire studies, suggesting that the sample device was able to collect gases predominantly

generated prior to ignition. Further evidence that ignition had not begun was corroborated by novel

IR detections of several species, in particular naphthalene. With regards to oxygenated species,

several aldehydes (acrolein, furaldehyde, acetaldehyde, formaldehyde) and carboxylic acids

(formic, acetic) were all observed; results show that ERs for acetaldehyde were noticeably greater

while ERs for formaldehyde and acetic acid were lower compared to other studies. The acetylene-

to-furan ratio also suggests that high temperature pyrolysis was the dominant process generating

the collected gases.

1. INTRODUCTION

Biomass burning contributes large quantities of trace gases into the earth's atmosphere (Crutzen and Andreae, 1990; Akagi et al., 2011; Andreae and Merlet, 2001; Crutzen et al., 1979; Yokelson et al., 2013; Andreae, 1991). The primary carbon-containing gases emitted during such burns are CO_2, CO and CH_4, in order of decreasing concentration (Ward and Hardy, 1991). Hundreds of other trace gases have also been identified in the emissions, including many non-methane volatile organic compounds (NMVOCs), oxygenated volatile organic compounds (OVOCs), nitrogen-containing species and sulfur compounds (Yokelson et al., 1996; Lobert et al., 1991; Talbot et al., 1988). The major sources of such biomass burning emissions are wildland fire and, to a lesser extent, prescribed fire. Prescribed fires are used to reduce dangerous fuel buildups and manage habitats (Fernandes and Botelho, 2003). The use of prescribed fire as a preventative tool is of particular importance in the western United States (U.S.) where wildland fires are increasing in severity (Turetsky et al., 2011; Miller et al., 2009). In the southeastern U.S., prescribed fire is also used on a routine basis for purposes such as ecosystem management (Waldrop and Goodrick, 2012). For these and other beneficial reasons, an estimated 3.6 million hectares of forestry land are burned in the U.S. by prescribed fire each year (Melvin, 2012). Agencies that conduct such burns often rely on fire-related models (Reinhardt et al., 1997; Prichard et al., 2006) to predict the impacts of the prescribed burn. Models and experience are used to determine desired fire behavior from fuel, weather, and topography in order to achieve the desired burn effects. The current operational model to predict fire behavior uses a simplistic approach to the chemical aspects of combustion and fire spread (Albini, 1976; Rothermel, 1972). Physics-based fire behavior models, while not currently fast enough for operational use, have the ability to incorporate details of fire behavior including heat transfer and chemical reactions (Clark et al., 2010; Mell et al., 2009). These models, such as FIRETEC and FDS, often model the process of pyrolysis based only on

54 results for wood or ground foliage samples. In order to improve the modeling of pyrolysis and

55 combustion processes for such models, a study is currently underway (Weise et al., 2018) wherein

56 pyrolysis products from the same plant species are being measured 1) in oxygen-free environment

57 using intact foliage samples (Amini et al., 2019a; Amini et al., 2019b; Safdari et al., 2019; Safdari

58 et al., 2018), 2) in an atmospheric oxygen wind tunnel setting with relatively simple heterogeneous

59 fuel beds (paper in preparation), and 3) in small field burns as discussed in this paper. One of the

60 goals of the larger study is to determine the relationship between the controlled laboratory results

61 and actual fire conditions in the field as was done previously by Yokelson et al. (2013); they

62 conducted a lab-field comparison study focusing mostly on the flaming and smoldering stages.

63 The present study focuses only on early stage emissions, particularly pyrolysis, in the hope that

64 improved elucidation of the gas-phase pyrolysis products and other early-stage processes of

65 prescribed burns will ultimately improve the overall ability to model fire behavior (Ferguson et

66 al., 2013; Shotorban et al., 2018; Yashwanth et al., 2016).

67

68 In the broader community, there has also been considerable interest in identifying and quantifying

69 gas emissions from fire due to the influential role of (wildland) fire on atmospheric chemistry and

70 climate, as studied both in the laboratory and in field burns (Crutzen et al., 1979; Andreae et al.,

71 1988; Lobert et al., 1991; Andreae et al., 1994; Lindesay et al., 1996; Goode et al., 1999; Yokelson

72 et al., 1999; Yokelson et al., 1996; Chi et al., 1979). The type of gases emitted and their relative

73 abundances depend on many factors such as fuel type, fuel arrangement, land management

74 activities, burning techniques and environmental conditions (Ward et al., 1996; Ward et al., 1992).

75 In the 1990s, Griffith, Yokelson and co-workers conducted a series of laboratory studies using an

76 open-path Fourier transform infrared (FTIR) spectrometer to investigate how some of these factors

77 influence the concentrations of emitted gases (Goode et al., 1999; Yokelson et al., 1996; Yokelson

78 et al., 1997). There have been several follow-on laboratory studies using IR spectroscopy as well

79 as other analytical techniques to identify previously unknown fire emission products and to derive

80 emission factors from various fuel types (Burling et al., 2010; Hatch et al., 2017; Selimovic et al.,

81 2018; Stockwell et al., 2014; Yokelson et al., 2013; Gilman et al., 2015).

82

83 In addition to those laboratory studies, a number of field campaigns have also used FTIR

84 spectroscopy to identify trace gases from prescribed fires (Akagi et al., 2013; Burling et al., 2011;

85 Akagi et al., 2014; Goode et al., 2000; Yokelson et al., 1999; Wooster et al., 2011; Alves et al.,

86 2010; Hurst et al., 1994a; Hurst et al., 1994b; Paton-Walsh et al., 2010; Paton-Walsh et al., 2008;

87 Guérette et al., 2018). Studies that have the ability to measure emissions both near the fire and

88 aloft are especially useful in understanding the complex chemistries that occur during and after

89 prescribed fires, including the (oxidative) chemistry of the downwind plume. For example, Akagi

90 et al. (2013) detected limonene from a prescribed burn with a land-based FTIR and linked it to the

91 production of ozone, formaldehyde and methanol, all of which were measured downwind with an

92 airborne-based FTIR. In an earlier prescribed burn study, (Burling et al., 2011) detected enhanced

93 levels of isoprene and 1,3-butadiene in the smoke from a living tree when compared to dead stumps

94 under the same conditions. However, pre-flame pyrolysis emissions can be relatively low

95 compared to total emissions from a fire, and few investigations have studied the pre-ignition or

96 pyrolysis gases emitted prior to the flaming combustion stage. Pyrolysis, which is one of the first

97 steps in the burning process (Collard et al., 2014), leads to char formation, depolymerization and

98 species fragmentation. Volatile products are generated and, if unstable, can continue to undergo

99 secondary (non-combustion) reactions such as cracking or recombination (Collard and Blin, 2014).

100   Pyrolytic reactions produce fuel gases that, if sufficient in quantity and in the presence of oxygen,

101   will maintain the flame via combustion pathways (Ward and Hardy, 1991; Di Blasi, 1993).

102

103   While there are few field studies of pyrolysis, there have been many laboratory studies carried out

104   in controlled environments: In one of the earliest investigations, DeGroot et al. (1988) detected

105   H_2O, CO_2, CH_3OH, HCOOH and CH_3COOH from the pyrolysis of wood. More recent studies

106   have observed several other compounds, such as CO, CH_4, lightweight hydrocarbons (C_2–C_5) and

107   light tar compounds (e.g. benzene and its derivatives and polycyclic aromatic hydrocarbons) from

108   the slow pyrolysis of Birch wood (Fagernäs et al., 2012). Oxygenated compounds (e.g. furan-

109   related compounds) have been observed from the fast pyrolysis of levoglucosan, a known

110   pyrolyzate of cellulose (Bai et al., 2013). Laboratory experiments that have investigated the

111   condensed and/or gas phase compounds generated by pyrolysis under controlled conditions have

112   revealed that the speciation and distribution of the products are dependent on a number of factors

113   such as heating rate, temperature, fuel composition, live vs. dead fuels and amount of available

114   oxygen (Azeez et al., 2011; Lu et al., 2011; Shen et al., 2010; Safdari et al., 2018; Ren and Zhao,

115   2012, 2013b, a). For instance, Ren and coworkers (2013a) found that the amount and speciation

116   of nitrogen containing pyrolyzates is complicated and influenced by the content of mineral matter,

117   the presence of oxygen (Ren and Zhao, 2012), as well as the structure (e.g. aliphatic vs.

118   heterocyclic) of the amino acids and the amount of cellulose, hemicellulose and lignin in the

119   sample. Similarly, the release of oxygenated compounds (e.g. phenolic compounds) from the

120   pyrolysis of lignin is sensitive to the presence of oxygen (Kibet et al., 2012).

121

122   All the above pyrolysis studies, however, were conducted in controlled settings or on smaller

123   scales. There remains a paucity of data that identify and quantify gas-phase pyrolysis species

124   emitted from actual prescribed burns at the field scale. The present study differs from these earlier

125   works in that we exclusively attempt to investigate gas-phase pyrolysis species generated during

126   prescribed burns. To the best of our knowledge, this is one of the first field studies that

127   discriminatively measures pyrolysis and early-phase gases for southeastern U.S. fuels. Isolating

128   such species is indeed challenging as they often blend with the background atmosphere and are

129   rapidly mixed with other gases from the onset of combustion. One must thus isolate "the pyrolysis

130   molecules" either optically, mechanically or temporally. In this study, we selectively probe the

131   pyrolysis gases by using a simple manually-operated spatial collection device that attempts to

132   collect only gases in front of the flame. While not a perfect solution, the information gathered in

133   this study adds important insights into the primary products generated during pyrolysis and other

134   early-stage processes for prescribed fires.

135

136

137   **2. EXPERIMENTAL**

138   **2.1 Site description**

139   During the week of 29 April 2018, a total of seven small plots (450 to 900 m^2) were burned using

140   prescribed fire at Ft. Jackson, South Carolina (SC), 34.05° N 80.83° W, approximately 10 km east

141   of Columbia, SC. The fort lies entirely within the Sandhills ecosystem in the SC coastal plain,

142   which runs approximately parallel to the Atlantic Ocean coast, 175 km inland. The Sandhills

143   region thus forms a belt that tracks southwest – northeast across sands of varying depth with a high

144   content of pure silica (Porcher and Rayner, 2001). The deep sands support an overstory vegetation

145 that has significant amounts of turkey oak (*Quercus laevis* Walter) and two native pine species

146 relatively unique to the southeastern U.S.: longleaf pine (*Pinus palustris* Mill.) and slash pine

147 (*Pinus elliottii* Engelm.). The understory has substantial quantities of immature turkey oak,

148 longleaf and slash pine, along with sparkleberry (*Vaccinium arboreum* Marshall) and a

149 heterogeneous organic layer of woody material, litter, duff and cones atop the mineral soil. The

150 longleaf ecosystem depends on fire for maintenance (Cary, 1932). Site details for the seven burn

151 plots, all with a 2 year rough (i.e. burned 2 years prior), are summarized in Table 1. Eight pre- and

152 post-fire 1.0 meter square biomass clipped plots were established at each 160 m^2 research block

153 within the larger burn plots where organic vegetative material was collected before and after each

154 fire. Shrub, grasses/forbs, down woody material (0-0.6, 0.6-2.5, 2.5-7.6, 7.6-22.9 cm in diameter),

155 litter and duff are the major fuel bed components that were targeted. Fuel moisture samples for

156 each major component were collected before ignition to determine fuel moisture content for each

157 fuel bed component. Figure 1 shows photographs of site 16, plot 1 before, during and after the

158 burn as well as a thermal image of the flame interacting with the fuel.

159
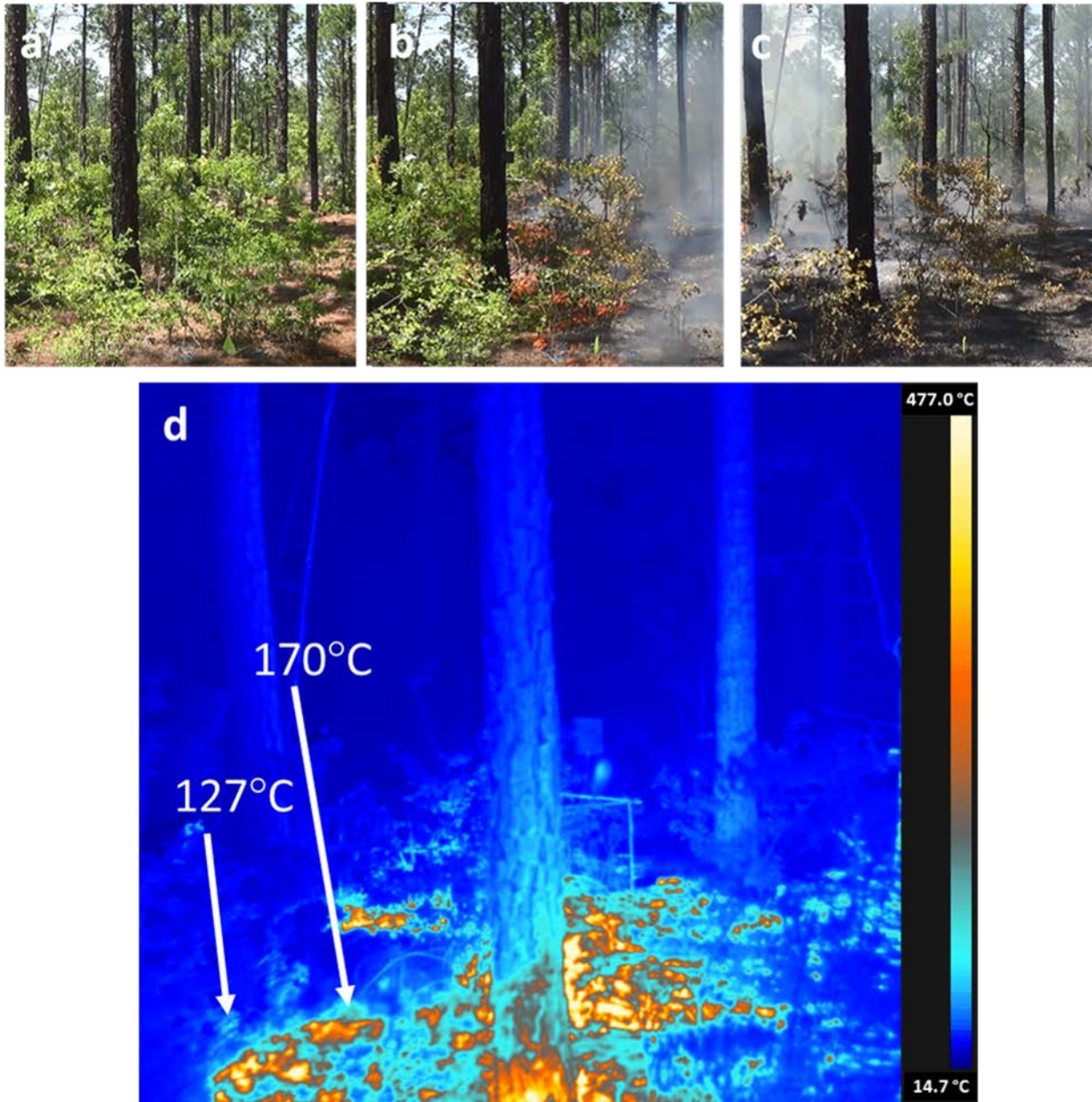
160
161
162 **Figure 1.** Photographs of site 16, plot 1 on 3 May 2018 between 14:00 and 14:40 local time. The plot (a) before the
163 flame, (b) while the flame interacted with the fuel at 14:33 and (c) smoldering combustion of the fuel. The primary
164 species seen in the understory for this burn plot are sparkleberry and a litter layer of pine needles. (d) Thermal image
165 of the flame interacting with the fuel at time of 14:33.
166
167

Table 1. Plot name, date/time, fuel description, atmospheric conditions (all clear sky days), and area for the prescribed burns.

Burn plot	Date (2018)	Local start time (EDT)	Local finish time (EDT)	Dominant overstory	Understory fuels	Ambient temperature (°C)	Relative humidity (%)	Surface winds (m s^{-1}) and wind direction	Mixing height (m)	Area burned (m^2)
24B-triangle	1-May	12:11	12:37	slash pine	sparkleberry/ logs	24	26	2.7 SW	975	450
24B-north diamond	1-May	13:53	14:43	slash pine	sparkleberry/ logs	28	18	2.7 SW	1310	900
24A-square	2-May	9:37	10:22	longleaf pine	sparkleberry/ duff	21	53	2.7 SW	792	900
24A-triangle	2-May	12:08	12:43	longleaf pine	sparkleberry/ duff	27	34	2.7 SW	1189	450
16 plot 5	3-May	9:39	10:21	longleaf pine	sparkleberry/ bracken fern	22	59	2.7 SW	579	900
16 plot 6	3-May	11:44	12:13	longleaf pine	sparkleberry/ turkey oak	26	43	3.1 SW	1067	900
16 plot 1	3-May	13:56	14:41	longleaf pine	sparkleberry/ turkey oak	29	30	3.1 SW	1494	900

2.2 Collection device

Our approach to sampling used an extractive collection device whose tube inlet sampled air and

emissions directly ahead of the flame. This simple solution is similar to other canister methods

often used with gas chromatographic analysis (Young et al., 1997) and also conceptually similar

to the land-based FTIR used to sample emissions as described by Akagi et al. (2013, 2014) and

Burling et al. (2011). The canister sampling package, mounted on a metal frame, contained a set

of evacuated canisters which were carried to the individual burn plots. The sampling package

consisted of a 12-Volt Swing Piston KNF Neuberger Pump (NPK09DC) plumbed with stainless

steel tubing and a pressure relief valve to regulate the pressure of the system and ultimately the fill

pressure of the canisters. The flow rate to fill the canisters was 15 liters min^{-1}. A sampling probe

(2.5 m of 6 mm stainless steel tubing plus 2 m of flexible stainless-steel line) was attached to the

inlet of the package to collect pyrolysis gases from point sources of vegetation within the burning

plots. The device had an in-line two-way valve to control the sampling interval. To capture a

pyrolysis sample, the probe was placed near the base of the flame, immediately above the fuel

188   where the pyrolysis gases should be emitted at maximal levels. Seven to ten aliquots of gas sample

189   were added to a single canister as the device was moved in front of the flame to capture pyrolysis

190   gases. Each 3-liter Summa canister was filled to approximately 138 kPa (20 psia) for the FTIR

191   analysis.

192

193   **2.3 FTIR spectrometer and spectral analysis**

194   Experimental details regarding FTIR measurement and ensuing spectral analysis procedures have

195   been previously reported (Scharko et al., 2019), but are briefly summarized as follows: Gases in

196   the canisters were returned from the field to the laboratory and analyzed the same day or the

197   following day using an 8 meter White cell (Bruker A136/2-L) and FTIR; canisters were connected

198   to the gas cell via 3/8" stainless steel tubing with both the tubing and gas cell heated to 70 °C to

199   prevent analyte adhesion. The cell was coupled to a purged FTIR spectrometer (Bruker Tensor 37)

200   equipped with a glow bar source, KBr beamsplitter and liquid-N_2-cooled mercury cadmium

201   telluride detector. Spectra were collected from 4000 to 500 cm^{-1} at 0.6 cm^{-1} resolution. Spectral

202   analysis was carried out using the MALT5 program (Griffith, 2016) and 50 °C reference spectra

203   from the PNNL database (Sharpe et al., 2004; Johnson et al., 2010) as well as absorption lines

204   from HITRAN (Gordon et al., 2017). MALT5 fits the assigned reference spectral lines to the

205   measured spectrum by optimizing the fit of all gases ascribed to the spectral window and

206   minimizing the residual. The calculation involves input parameters such as path length, resolution

207   and apodization accompanied by reference absorption cross-sections and the measured spectrum

208   with its associated temperature/pressure values. Both H_2O and CO_2 had peaks that were saturated;

209   these regions were eliminated from analysis. In some instances, peaks for the gases of interest were

210   also saturated in which case the pressure in the gas cell was reduced and the measurement repeated.

2.4 Calculation of emission ratios and emission factors

A convenient quantity to compare emissions is the emission ratio (ER). This ratio is calculated by computing the change in the concentration of analyte of interest relative to that of a co-emitted, long-lived gas, typically CO or CO_2. For the present study, the long-lived gas chosen is CO:

$$ER = \left(\frac{\Delta analyte}{\Delta CO}\right). \tag{1}$$

It is important to note that these are the changes in analyte and CO relative to background atmosphere (i.e. relative to ambient "clean air" conditions). The background levels of CO and CO_2 were measured using an open path gas analyzer (OPAG 22) prior to the series of burns. The initial CO_2 level was measured to be 409 ppm (this value agrees with the global averaged CO_2 for May 2018 of 408.7 ppm (Dlugokencky and Tans)) whereas the CO level was often below the OPAG detection limit. [Due to challenging experimental conditions and moderate CO band intensities, the OPAG detection limit was poor for these CO measurements and could not achieve 200 ppb.] Without an instrument to measure ambient CO with sufficient sensitivity we chose 200 ppb for an estimated background level which is within the range for a typical CO mixing ratio (Seinfeld and Pandis, 2012). We note that the 200 ppb value is sufficiently small that it has negligible effect on the calculated $\Delta analyte/\Delta CO$ ratios. Emission ratios can be calculated for a single point in time during the fire or they can incorporate the full length of the fire. The present ERs were calculated based on the contents of the individual canisters which represent multiple aliquots, all from the early fire stages. Other studies have obtained fire-integrated ERs, which integrate over the entire duration of the fire (Koss et al., 2018) or fire-averaged ERs determined from the slope of the regression with the intercept set to zero (Yokelson et al., 1999).

232 Another useful quantity is the emission factor (EF), defined as the number of grams emitted of a

233 given analyte per kilogram of dry fuel consumed and estimated using the following equation

234 (Yokelson et al., 1999; Ward and Radke, 1993):

$$\text{EF (g kg}^{-1}) = F_{carbon} \times 1000 \times \frac{MW_{analyte}}{MW_{carbon}} \times \frac{\dfrac{\Delta analyte}{\Delta CO_2}}{\sum_{j=1}^{n}\left(NC_j \times \dfrac{\Delta C_j}{\Delta CO_2}\right)}$$

235

(2)

236

237 where F_{carbon} is the mass fraction of carbon in the fuel, $MW_{analyte}$ and MW_{carbon} are the molar masses

238 of the analyte and carbon, respectively, $\frac{\Delta analyte}{\Delta CO_2}$ is the emission ratio of the analyte relative to CO_2,

239 $\frac{\Delta C_j}{\Delta CO_2}$ is the emission ratio of species j relative to CO_2 and NC_j is the number of carbons in species

240 j. Note that ΔCO_2 cancels out in equation 2. Elemental analysis of similar southeastern fuels was

241 reported in a previous study (Safdari et al., 2018), and the average carbon content by mass for

242 longleaf pine foliage and litter as well as sparkleberry was 0.52 which was the value used for

243 F_{carbon}. One assumption in equation 2 is that all of the carbon in the fuel is released and accounted

244 for in the measurements of the j carbon species. Most carbon emissions are in the chemical form

245 of CO_2, CO or CH_4. It should be noted that the EF quantities reported here include only compounds

246 measured by the FTIR, and EF values may be overestimated by 1-2% for most fuels due to

247 undetected carbon species (Akagi et al., 2011).

248

249 **3. RESULTS AND DISCUSSION**

250 **3.1 Estimating the contribution from high and low temperature processes**

251 Modified combustion efficiency (MCE) uses the excess CO and CO_2 values to quantify the degree

252 of combustion that has occurred in a given smoke plume and the MCE will be discussed below.

253 However, in a recent study Sekimoto et al. (2018) suggested that MCE may not be the best quantity

254 to adequately describe pyrolysis, but rather that emissions of volatile organic compounds (VOCs)

255 from biomass burning may be correlated with high and low temperature pyrolysis factors obtained

256 by carrying out positive matrix factorization (PMF) analysis on the emission profiles. The authors

257 further suggested that the ratio of acetylene (C_2H_2) to furan (C_4H_4O) could be used to estimate the

258 high and low temperature pyrolysis factors. They used the emission profiles from the analysis of

259 15 different fuels to calculate the following ratio that estimates the high and low temperature VOC

260 emissions:

$$\frac{(\text{Total VOC})_{\text{High T}}}{(\text{Total VOC})_{\text{Low T}}} = \frac{C_2H_2 \; / \; 0.0393}{C_4H_4O \; / \; 0.0159}. \tag{3}$$

261 We have adopted this estimation approach and have used the acetylene-to-furan ratio to assess the

262 relative contributions from high and low temperature processes. The average results are displayed

263 in Figure 2 alongside the results from Koss et al. (2018), Gilman et al. (2015) and Akagi et al.

264 (2013). For comparison purposes, the values displayed in Figure 2 were determined using average

265 ERs for acetylene and furan. The present results (right-most bar) are approximately an order of

266 magnitude greater than all previous studies, likely due to the timing of collection and the sampling

267 probe's proximity to the flame. The juxtaposed values from the previous studies were obtained

268 using either a) fire-integrated ERs, b) discrete ERs sampled every 20 to 300 sec or c) fire-averaged

269 ERs, all of which incorporate several different phases of the fire as compared to the present flame-

270 front measurements. Using the Sekimoto et al. (2018) estimation approach, higher acetylene-to-

271 furan ratios indicate a greater contribution from the high temperature process. The markedly high

272 ratio observed in this study suggests that samples were collected when high temperature pyrolysis

273 was indeed the dominant process. This observation is consistent with the time profile for the

274 contribution of the high temperature pyrolysis factor presented by Sekimoto et al. (2018), which

275 demonstrates that the contribution from high temperature pyrolysis [High-T / (High-T + Low-T)]

276 can easily exceed 0.95 in the early stages of fire, but reduces to smaller fractions (≤ 0.3) in the

277 latter stages. Another key difference is that the sampling probe used at Ft. Jackson was positioned

278 so as to extract gases directly before the flame front, yet in close proximity to it, in order to limit

279 further reactions. In particular, if the highly flammable acetylene molecules were captured prior to

280 subsequent oxidation reactions, this would explain the enhanced ratio of high-to-low-temperature

281 VOC emissions as seen in Figure 2.
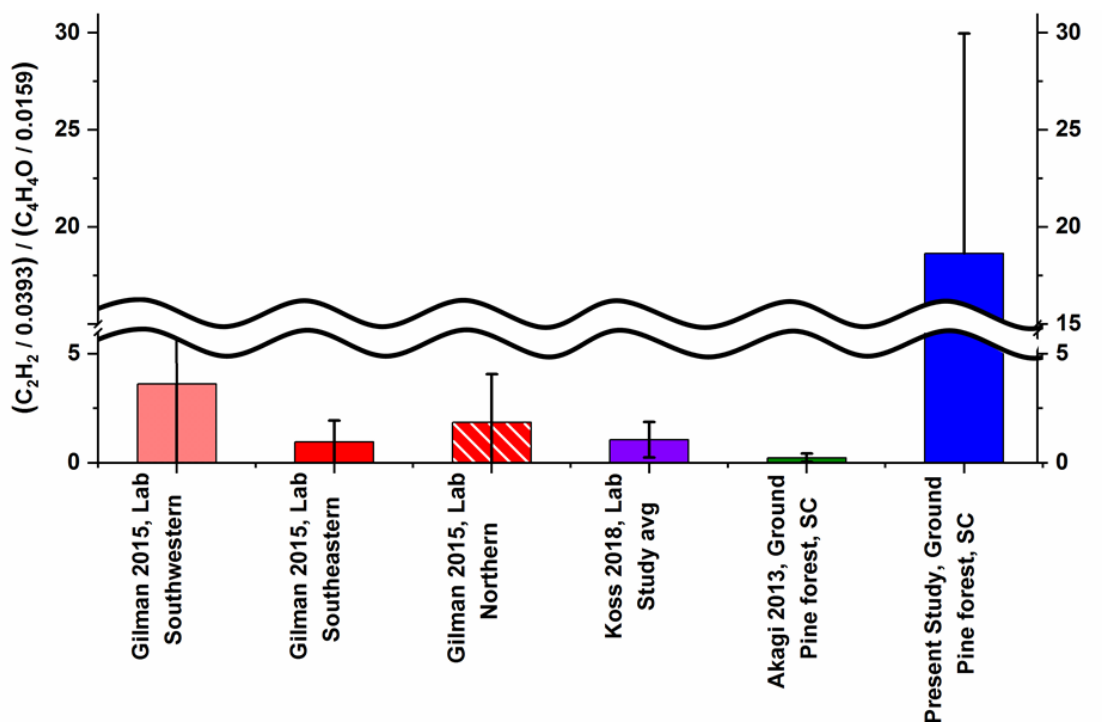
282

283 **Figure 2.** Ratio of acetylene (C_2H_2)/0.0393 to furan (C_4H_4O)/0.0159 to predict the ratio of high to low temperature
284 VOC emissions as outlined by Sekimoto et al. (2018). Error bars represent 1σ. For the present study average results
285 were determined from the 10 collected samples preceding the flame front for acetylene and furan. Koss et al. (2018)
286 values were fire integrated while Gilman et al. (2015) used 20-300 sec integrations. Akagi et al. (2013) reported EFs
287 which were used to calculate ERs for acetylene and furan.

3.2 CO_2 and CO emissions and MCE values

As expected, other than H_2O vapor, CO and CO_2 were the predominant gases observed as emissions. Table 2 displays the EF (g kg^{-1}) and ER (ppb/ppm$_{CO}$) values averaged for the ten field measurements. Most prescribed burn studies have focused only on the flaming and smoldering stages. The flaming stage is characterized by more oxidized products and a higher modified combustion efficiency (e.g. 0.85 - 0.97, even 0.99 for pure flaming) (Ward and Hao, 1991), where the MCE is defined as:

$$MCE = \left(\frac{\Delta CO_2}{\Delta CO_2 + \Delta CO}\right).$$

(4)

The smoldering phase with lower MCE values (typically ranging from 0.65–0.85) (Urbanski, 2013) displays more non-oxidized (or less-oxidized) species but with a greater fraction of OVOCs observed. The arithmetic mean MCE and standard deviation for all ten measurements at Ft. Jackson was 0.83 ± 0.04. Such MCE values would normally characterize data gathered during smoldering combustion where a combination of processes such as pyrolysis along with glowing combustion of char take place (Yokelson et al., 1997). Since the present study was aimed at collection of pyrolysis gases preceding the flame front, characterizing the results in terms of MCE values may not be appropriate: The lower MCE values do not represent the fire being in the smoldering stage, but rather suggest that pyrolysis and other early-phase process gases were captured (at least in part) prior to the onset of combustion. As noted, the methodology used with this collection device ideally extracts the pyrolysis gases before they are combusted. Due to the proximity of these gases to the flame, some entrainment of ambient air and air from the flame region was likely unavoidable. As we were sampling a moving zone, some combustion products were also likely to be sampled.

Table 2. Study averages of EF (g kg^{-1}) and ER (ppb/ppm$_{CO}$) for the ten pyrolysis measurements along with standard deviation (SD). The SD represent the variation for the ten non-identical measurements. For the study averages, the arithmetic mean MCE was found to be 0.83 ± 0.04.

Species	Formula	EF Study Average (g kg^{-1})	SD	ER Study Average (ppb/ppm$_{CO}$)	SD
Carbon dioxide	CO_2	1469	113	5190	1450
Carbon monoxide	CO	191	45	1000	n/a
Methane	CH_4	11.2	3.9	101.3	18.7
Ethane	C_2H_6	1.14	0.42	5.54	1.48
Ethene	C_2H_4	11.8	3.8	61.1	9.6
Acetylene	C_2H_2	7.4	3.1	40.9	10.4
Propene	C_3H_6	2.69	1.04	9.32	2.34
Allene	C_3H_4	0.30	0.12	1.09	0.23
1,3-Butadiene	C_4H_6	1.20	0.72	3.13	1.25
Isobutene	C_4H_8	0.23	0.15	0.58	0.31
Isoprene	C_5H_8	0.63	0.90	1.18	1.43
Naphthalene	$C_{10}H_8$	0.65	0.36	0.77	0.47
Formaldehyde	HCHO	0.76	0.98	3.63	4.57
Methanol	CH_3OH	1.39	1.40	6.11	5.56
Formic acid	HCOOH	0.23	0.14	0.74	0.42
Acetaldehyde	CH_3CHO	2.84	1.41	9.35	3.59
Acetone	$(CH_3)_2CO$	1.15	0.77	2.92	1.78
Acetic acid	CH_3COOH	1.45	2.66	3.46	6.15
Acrolein	C_3H_4O	1.59	1.01	4.10	2.15
Furan	C_4H_4O	0.41	0.25	0.89	0.49
Furaldehyde	C_4H_3OCHO	1.01	1.01	1.45	1.31
Hydrogen cyanide	HCN	1.34	0.31	7.34	1.25
Nitrous acid	HONO	0.10	0.16	0.30	0.46
Methyl nitrite	CH_3ONO	0.41	0.32	1.06	0.90

3.3 Emissions of lightweight hydrocarbons

Besides CO and CO_2, the second most abundant class of gases generated during the prescribed burns was lightweight hydrocarbons (HCs). The lightweight HCs detected by the FTIR include methane, ethane, ethene, acetylene, propene, allene, 1,3-butadiene, isoprene and isobutene. Most

318   have been previously identified in fire emissions using FTIR either in laboratory experiments

319   (Burling et al., 2010; Christian et al., 2003; Christian et al., 2004; Gilman et al., 2015; Goode et

320   al., 1999; Hatch et al., 2017; Selimovic et al., 2018; Stockwell et al., 2014; Yokelson et al., 1996;

321   Yokelson et al., 1997) or field settings (Akagi et al., 2013; Akagi et al., 2014; Alves et al., 2010;

322   Burling et al., 2011; Goode et al., 2000; Hurst et al., 1994a; Hurst et al., 1994b; Karl et al., 2007;

323   Paton-Walsh et al., 2010), but the present experiment reports the first IR detection of allene

324   (Scharko et al., 2019). Figure 3 shows the individual correlations between these lightweight HCs

325   and excess CO mixing ratios. The analyte vs. ΔCO correlation coefficients range from 0.97 (ethene

326   and allene) to 0.66 (isoprene and isobutene). In all cases, the correlation coefficients were larger

327   with CO than with CO_2. Positive relationships have been observed for CO correlations in previous

328   burning studies (Hurst et al., 1994a; Hurst et al., 1994b).
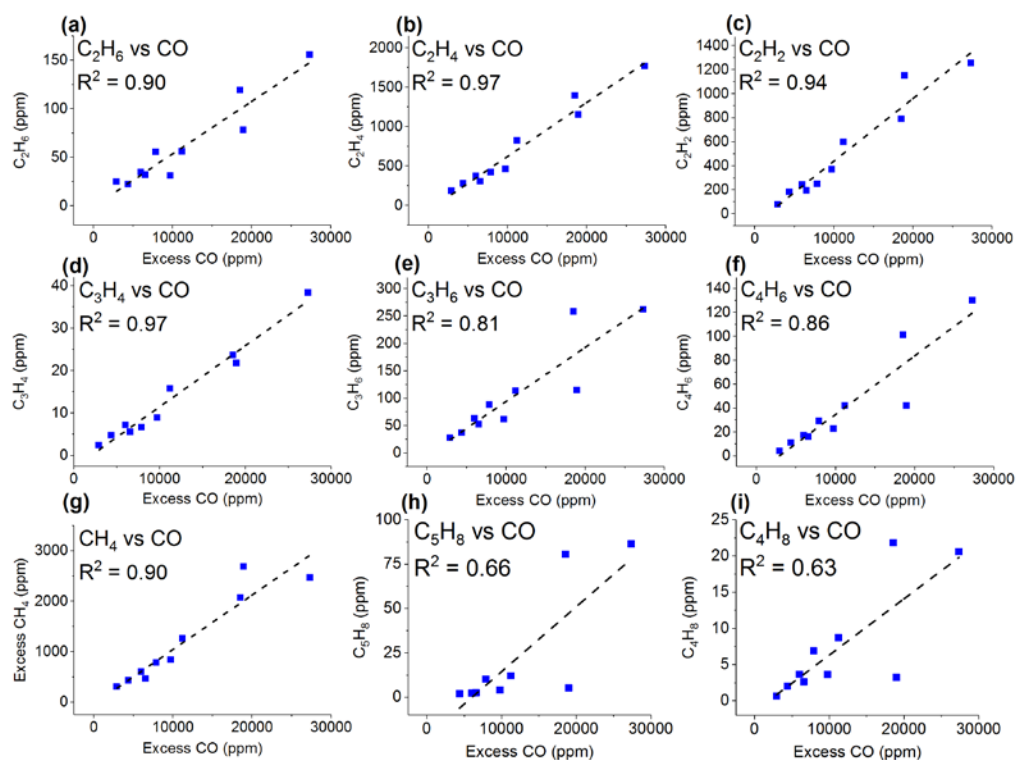
329

330   **Figure 3.** Mixing ratios (ppm) for the 10 measurements as a function of excess CO (ppm) for (a) ethane (C_2H_6), (b)
331   ethene (C_2H_4), (c) acetylene (C_2H_2), (d) allene (C_3H_4), (e) propene (C_3H_6), (f) 1,3-butadiene (C_4H_6), (g) excess methane
332   (CH_4), (h) isoprene (C_5H_8) and (i) isobutene (C_4H_8). The dashed lines are a linear fit to the data.

333   While the observed ER for excess methane was comparable, ERs for ethene and acetylene were

334   considerably greater than previously reported values. Specifically, Figure 4 shows a comparison

335   of emission ratios for methane, ethene and acetylene to previously reported values of Gilman et al.

336   (2015) and Akagi et al. (2013). As noted, different sampling methods complicate the comparison.

337   The present data represent a collection of instantaneous grab samples extracted directly before the

338   flame front, whereas the other data represent time averaged values. Ethene and acetylene have both

339   been observed as pyrolysis products in prior laboratory work (Palma, 2013), but may react further.

340   For example, the addition reaction of acetylene to benzene or naphthalene can produce styrene or

341   cyclopenta-fused polycyclic aromatic hydrocarbons (Ledesma et al., 2002). Alternatively ethene

342   and acetylene can undergo combustion (Simmie, 2003). Nevertheless, the high ER values for

343   ethene and especially for acetylene in the present study further suggest that the samples were

344   collected when high temperature pyrolysis process was dominant; Sekimoto et al. (2018) also

345   observed that high temperature pyrolysis profiles are often associated with unsaturated

346   hydrocarbons.
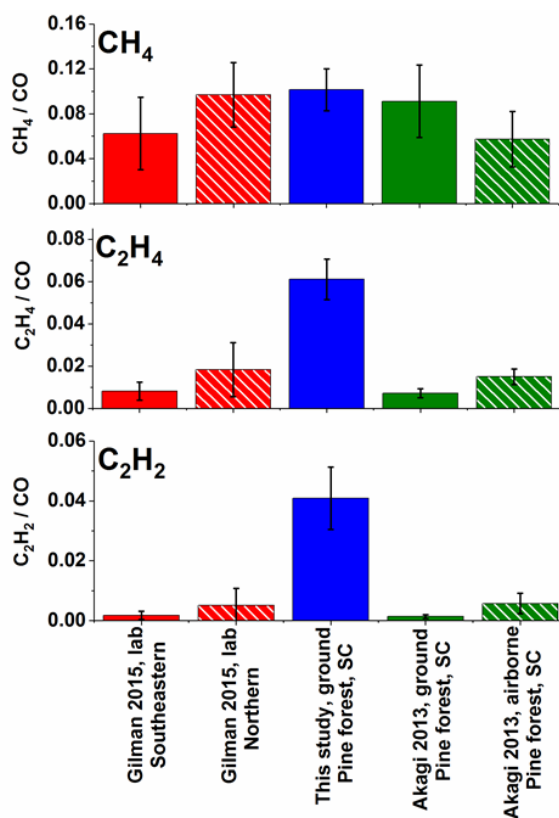
347
348
349 **Figure 4.** Average ERs (ppm/ppm$_{CO}$) for excess methane (top), ethene (middle) and acetylene (bottom) for this study
350 and for previously published laboratory and field (ground and air based) investigations. Error bars represent 1σ.
351 Gilman et al. (2015) present discrete ERs with sample acquisition of 20 to 300 sec. Akagi et al. (2013) present fire-
352 averaged EFs calculated using ERs derived by the regression method. The ERs for Akagi et al. shown above were
353 derived from the ratio of the EFs for the gas of interest and CO multiplied by the molar mass of CO/molar mass of
354 analyte.
355

356 **3.4 Emissions of lightweight oxygenated hydrocarbons**

357 The noncyclic oxygenated hydrocarbons detected via FTIR analysis include formaldehyde,

358 methanol, formic acid, acetaldehyde, acetone, acetic acid and acrolein. On average, acetaldehyde

359 and methanol had the highest ER values in this group, with ERs relative to CO of 0.009 and 0.006,

360 respectively, as seen both in Table 2 and Figure S2 in the supplemental material. For all

361 measurements collected at sites 16 and 24A, acetaldehyde was consistently the highest with ER

362 values ranging from 0.005 to 0.014. Site 24B followed a different trend with highest ER values for

363 acetic acid, followed by methanol, acetaldehyde and formaldehyde in decreasing order. The ERs

364 for acetic acid and formaldehyde at site 24B are at least 7.9 and 2.5 times greater, respectively,

365   than the other burn sites: One key difference observed for site 24B was fuel composition, namely

366   the presence and partial consumption of larger logs (i.e. 7.6–20.3 cm diameter woody material).

367   Other differences include the presence of live pine seedlings and fewer turkey oak as compared to

368   other plots. This particular plot had the highest herbaceous and forb pre-fire loading and

369   consumption with a higher fuel moisture content (205% as compared to next highest value of

370   144%). This high fuel moisture content was reflected in the ER for water, which was at least 4.7

371   times greater than the other plots. The pyrolysis of cellulose (one of the three primary components

372   of biomass as discussed below) forms levoglucosan. Shen et al. (2009) outline secondary

373   decomposition pathways for levoglucosan, in which the initial step is the rehydration to generate

374   glucopyranose. They demonstrate how glucopyranose can then form formaldehyde, methanol and

375   acetic acid via secondary decomposition routes. This pathway (or a similar one) may have been

376   favored at site 24B: the greater ERs for acetic acid and formaldehyde observed at plot 24B may

377   have thus been influenced by the greater fraction of woody material and presence of herbaceous

378   and forb fuels, all with higher moisture contents. This hypothesis warrants further investigation,

379   and could be studied in the laboratory.

380   Table 3 compares the present ER values with values from Akagi et al. (2013), Stockwell et al.

381   (2014), Gilman et al. (2015) and Koss et al. (2018). The present ERs are comparable to other burn

382   studies except for acetaldehyde, which appears to be marginally greater, and formaldehyde and

383   acetic acid, which both appear to be lower. The higher ratio for acetaldehyde may be due to

384   differences in the sampling approach, i.e. samples collected in the present study may contain

385   species that were generated during an earlier period in the thermal decomposition process. In a

386   controlled laboratory study by Stein et al (1983), acetaldehyde was observed as one of the initial

387   products emitted from the pyrolysis of glycerol, a product pyrolyzed from levoglucosan. This same

388 study also observed that acetaldehyde would continue to decompose (under pyrolysis conditions)

389 to smaller molecules such as ethene, methane, H_2 and CO (Stein et al., 1983). The greater average

390 ER for acetaldehyde observed in the present study may be due to gases being captured (via the

391 collection device) and removed from heat either in-between decomposition steps or before

392 combustion. It is also possible that the trends seen for the OVOCs in Table 3, in particular the

393 higher values for acetaldehyde arise due to (a) differing vapor pressures, (b) differing degrees of

394 onset of combustion, (c) differing degrees of pyrolysis emissivity as suggested by Stein et al.

395 (1983), (d) differing degrees of IR-spectroscopic sensitivity (i.e. certain other species with limited

396 or no detectivity), or (e) some combination of all these effects. Further analysis is warranted.

Table 3. Average emission ratios (ppb/ppm$_{CO}$) for this study and for previously published fire studies.

Analyte	This study-Pine forest SC ground-based	Gilman et al., 2015 Southeastern fuels	Koss et al., 2018 Study average for all fuels	Stockwell et al., 2014 Sawgrass SC	Stockwell et al., 2014 Ponderosa pine MT	Akagi et al., 2013 Pine forest SC ground-based	Akagi et al., 2013 Pine forest SC air-based
Formic acid	0.7	1.6	2.2	0.7	5.1	n/a	0.6
Furan	0.9	0.7	1.9	0.8	1.2	2.4	1.1
Furaldehyde	1.5	1.5	2.1	n/a	n/a	0.1	0.2
Acetone	2.9	1.6	2.3	n/a	n/a	3.8	3.6
Formaldehyde	3.6	12	20	7.8	29	12	23
Acetic acid	3.5	13	n/a	5.2	22	6.6	11
Acrolein	4.1	1.3	5.4	n/a	n/a	1.2	1.8
Methanol	6.1	7.8	12	3.4	24	21	13
Acetaldehyde	9.3	2.8	7.4	n/a	n/a	5.1	4.8

Koss et al. (2018) present the fire-integrated ERs. Gilman et al. (2015) present discrete ERs with sample acquisition of 20 to 300 sec. Stockwell et al. (2014) present the fire-integrated ERs. Akagi et al. (2013) present fire-averaged EFs calculated using ERs derived by the regression method. The emission ratios for Akagi et al. (2013) were obtained from the ratio of the emission factors for the analyte and CO multiplied by the molar mass of CO/molar mass of the analyte.

397

398 The slightly lower ERs for formaldehyde and acetic acid may in part be explained by secondary

399 decomposition pathways. Proposed pathways that generate formaldehyde and acetic acid proceed

400 through intermediates formed by the decomposition of levoglucosan (Shen and Gu, 2009).

401 Formaldehyde is generated from a number of intermediates such as hydroxyacetone (acetol)

402 (Lindenmaier et al., 2016) and 5-hydroxymethyl-furfural. While the formation mechanism for

403 acetic acid is via the decomposition of the intermediate hydroxyacetaldehyde (glycolaldehyde)

404 (Johnson et al., 2013), which undergoes a dehydration reaction to a ketene, and then a rehydration

405 to acetic acid (Shen and Gu, 2009), it is possible that the present conditions and fuels (save for site

406 24B) were not favorable for the above chemical pathways.

3.5 Emissions of aromatic compounds

408 In the present study, furan, furaldehyde and naphthalene were all detected via FTIR. Previous fire

409 studies have used FTIR to detect phenol and/or furan (Burling et al., 2011; Akagi et al., 2014;

410 Hatch et al., 2017; Christian et al., 2003; Christian et al., 2004; Stockwell et al., 2014; Karl et al.,

411 2007; Selimovic et al., 2018; Yokelson et al., 2013; Burling et al., 2010; Akagi et al., 2013). One

412 of these studies also detected furaldehyde (Selimovic et al., 2018). To the best of our knowledge,

413 however, this is the first burning study that has used IR spectroscopy to identify naphthalene vapor,

414 though it has previously been detected in biomass burning emissions via other methods (Koss et

415 al., 2018; Gilman et al., 2015). Naphthalene has also been detected in tar samples generated from

416 the controlled pyrolysis of similar fuels (Safdari et al., 2018).

417

418 Phenol and phenolic compounds were not definitively observed in this study due to their IR bands

419 being somewhat weak and obscured by a number of other species, namely acetic acid, carbon

420 dioxide, acetylene and hydrogen cyanide. However, phenolic compounds have been identified in

421 products generated from the pyrolysis of lignin in controlled laboratory experiments by Kibet et

422 al. (2012). Lignin, one of the three main components of biomass, can account for 10–35% of the

423 biomass, and its chemical structure consists of polymers of various phenolic alkyl side chain

424 subunits (Shen et al., 2015). When undergoing thermal decomposition, lignin will release volatiles

425 at temperatures between 200 and 400 °C. The proposed mechanism can generate intermediates

426 such as phenoxy radicals that ultimately lead to the formation of phenols (Kibet et al., 2012). In

427 the present study, spectral evidence of phenol was in fact observed in some measurements, but the

428 IR bands at 1176 and 752 cm^{-1} were weak and were masked by other compound signatures,

429 hindering spectral quantification. Mixing ratios of phenol above the detection limit might have

430 been anticipated since prior controlled pyrolysis investigations of sparkleberry and longleaf pine

431 have detected phenol as a component in the tar (Safdari et al., 2018; Amini et al., 2019a; Safdari

432 et al., 2019). While the phenol signal was weak, furan and furaldehyde, however, were clearly

433 detected, and their formation likely stemmed from thermal degradation of the other main

434 constituents of biomass. Besides lignin, the other primary macromolecular components are

435 cellulose and hemicellulose, which account for approximately 50% and 15–35% by weight,

436 respectively (Shen et al., 2015). The pyrolysis of cellulose is known to produce furaldehyde, furan

437 and other low weight oxygenated compounds (e.g. acetic acid) via the intermediate levoglucosan

438 (Bai et al., 2013). Moreover, furaldehyde and methanol have both been observed as volatile

439 products from the pyrolysis of methyl β-D-xylopyranoside, a model compound for xylan-based

440 hemicellulose (Shafizadeh et al., 1972).

441

442 Naphthalene is a polycyclic aromatic hydrocarbon with several sources including as a biomass

443 burning emission product. It was detected using FTIR for the first time in these studies (Scharko

444 et al., 2019). Its IR detection was not unexpected given that it has been observed in collected tar

445 samples generated by the laboratory pyrolysis of similar fuel types (Safdari et al., 2018) but its

446 identification in an experimental IR spectrum can be challenging as depicted in Figure 5. Most of

447 its IR bands have only moderate cross-sections with the exception of the ν_{46} band, which has a

448 strong Q-branch at 782.3 cm^{-1} (green trace in Figure 5). For this band to be observed, however, it

449 needs to be deconvoluted from the acetylene rotational-vibrational lines also present in this spectral

450 domain (red trace in Figure 5). Better retrievals for naphthalene were obtained using a higher

451 spectral resolution (0.6 cm^{-1}) since the Q-branch of the ν_{46} band is quite sharp (FWHM ~ 1 cm^{-1}),

452 even at atmospheric pressure (Scharko et al., 2019) .
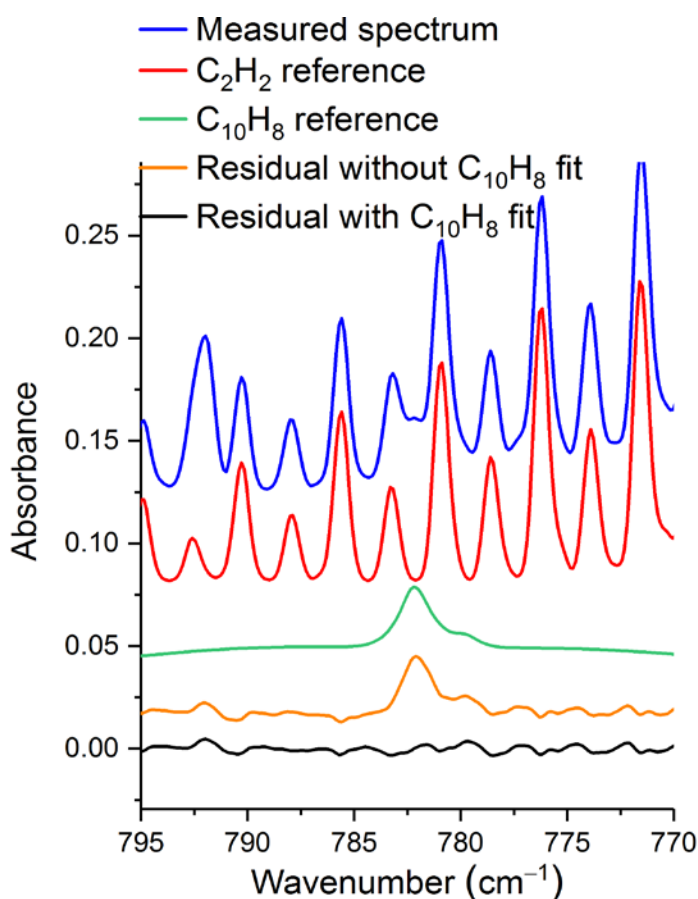
453

454 **Figure 5.** Measured and scaled reference spectra for acetylene (C_2H_2) and naphthalene ($C_{10}H_8$) as well as residual
455 with and without $C_{10}H_8$. The measurement is from site 16 plot 6 msmt. 2, and the detected mixing ratio for naphthalene
456 is 7.37 ppm. Spectra are offset for clarity. Reference absorption lines for acetylene are from HITRAN, and the
457 reference spectrum for naphthalene is from PNNL.

458 Figure 6a plots the mixing ratios (ppm) for naphthalene as a function of excess CO (ppm) while

459 Figure 6b displays the ERs for naphthalene for this study and previous studies.
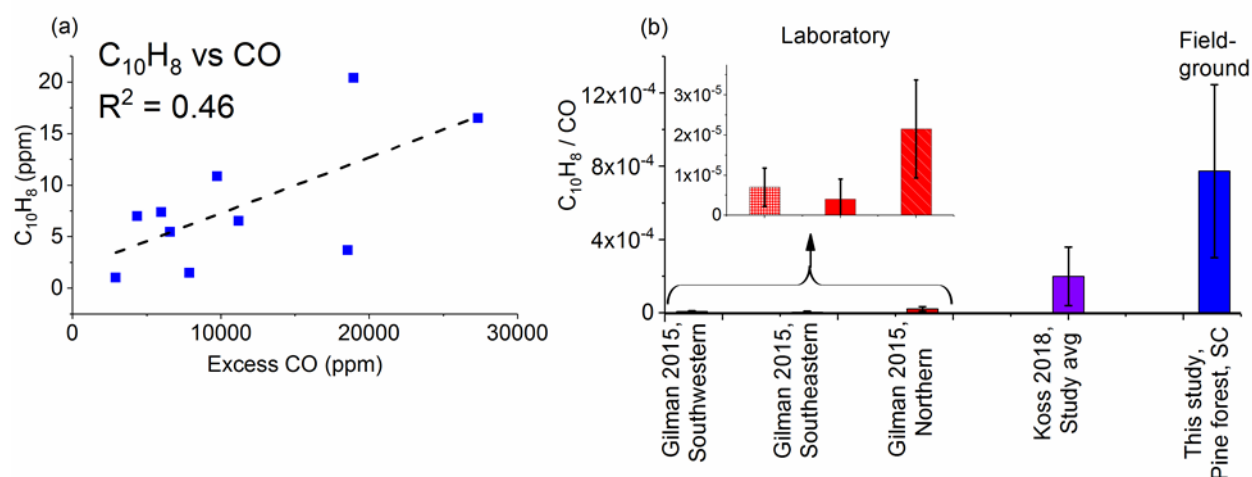
460
461 **Figure 6.** (a) Mixing ratios (ppm) for naphthalene ($C_{10}H_8$) as a function of excess CO (ppm) measured by FTIR for
462 each of the 10 canisters. The dashed line is a linear fit. (b) Average emission ratios ($ppm_{C_{10}H_8}/ppm_{CO}$) for this study
463 and for previous laboratory studies. Error bars represent 1σ. Koss et al. (2018) present the fire-integrated ERs. Gilman
464 et al. (2015) present discrete ERs with sample acquisition of 20 to 300 sec.
465

466   The average naphthalene ER for this study is substantially greater than both the values from

467   Gilman et al. (2015) and Koss et al. (2018). The average for Koss et al. (2018), however, is in turn

468   an order of magnitude greater than the highest average for Gilman et al. (2015). The higher ER

469   for naphthalene in this study (shown in Figure 6) clearly suggests that the method to capture

470   pyrolysis gases was (at least in part) quite successful, i.e. we were able to collect naphthalene gas

471   prior to it undergoing further reactions. Besides oxidation, under the right conditions naphthalene

472   can also continue to react in a Diels-Alder type reaction to form still larger polyaromatics (Fairburn

473   et al., 1990; Richter and Howard, 2000). Sekimoto et al. (2018) also linked naphthalene with the

474   high temperature profile, and it appears that the samples in the present study were indeed collected

475   when the high temperature process was dominant. The detection of naphthalene suggests that

476   benzene and/or styrene, which are the main precursors to polycyclic aromatic hydrocarbons, may

477   also be present. Styrene was not detected via FTIR methods, and benzene is challenging for IR

478 analysis since its one strong band (ν_{11} mode at 673 cm^{-1}) is obfuscated by the CO_2 ν_2 bending

479 mode under such polluted atmospheric conditions.

480

3.6 Emissions of nitrogen-containing species

482 Gases such as NH_3, NO_2, NO, HCN and HONO have been identified using FTIR spectroscopy in

483 fire laboratory experiments multiple times (Selimovic et al., 2018; Gilman et al., 2015; Christian

484 et al., 2003; Christian et al., 2004; Goode et al., 1999; Yokelson et al., 1996; Yokelson et al., 1997;

485 Stockwell et al., 2014; Hatch et al., 2017; Burling et al., 2010; Karl et al., 2007) as well as in field

486 studies (Yokelson et al., 1999; Burling et al., 2011; Goode et al., 2000; Akagi et al., 2013; Karl et

487 al., 2007; Akagi et al., 2014). Multiple other methods have also been used to detect N-containing

488 gases, such as HNCO and CH_3CN (Gilman et al., 2015; Christian et al., 2003; Christian et al.,

489 2004; Yokelson et al., 2009; Akagi et al., 2013; Karl et al., 2007; Roberts et al., 2010). The amount

490 and speciation of N-containing compounds emitted is dependent on fuel type and nitrogen content

491 (Stockwell et al., 2014; Burling et al., 2010; Coggon et al., 2016). Moreover, emissions can usually

492 be linked to a stage of combustion: NO, NO_2, HNCO and HONO are all associated with the

493 flaming stage, while NH_3 and HCN are primarily associated with smoldering combustion but have

494 also been suggested as pyrolysis gases (Goode et al., 1999; Yokelson et al., 1996; Roberts et al.,

495 2010; Burling et al., 2010; Hansson et al., 2004; Di Blasi, 2008). Biomass pyrolysis experiments

496 carried out in an inert (i.e. oxygen free) atmosphere have revealed that NH_3, HCN and HNCO are

497 all generated (Hansson et al., 2004). These compounds are all considered to be NO_x (NO + NO_2)

498 and N_2O precursors because they are oxidized via combustion (Hansson et al., 2004).

499 It is important to note that ammonia and related amine compounds are often best sampled via open-

500 path techniques such as an open White Cell, as these compounds are notorious for adhering to

501 walls of sampling or analysis devices, including those made from steel, glass or Teflon (Stockwell

502 et al., 2014; Yokelson et al., 2003). Sampling and passivation techniques have been discussed

503 extensively (Neuman et al., 1999; Roscioli et al., 2015) for these "sticky" molecules, and the

504 present method may thus not be optimal for these compounds. This caveat in mind, the major N-

505 containing compound that was identified in the present pyrolysis study was HCN. This is

506 consistent with previous small-scale and controlled laboratory studies that have shown HCN as

507 the primary N-product resulting from the pyrolysis of amino acids (Haidar et al., 1981; Johnson

508 and Kan, 1971). This observation is further evidence that the gas samples were extracted when

509 high temperature was the dominant process; Sekimoto et al. (2018) have associated HCN with the

510 high temperature pyrolysis profile. Figure 7a shows the correlation between HCN and excess CO

511 (R^2 = 0.89). Previous field fire studies have observed similar trends (Simpson et al., 2011;

512 Stockwell et al., 2016). Figure 7b shows a comparison between the ERs for HCN for this study as

513 well as from previous laboratory and field (both ground and airborne) studies. The present values

514 are comparable to other ground-based measurements (Guérette et al., 2018; Akagi et al., 2013) but

515 differ significantly from a couple of the laboratory studies. It should be noted that although

516 conducted at a different time of the year (late Oct./early Nov. 2011), the studies by Akagi et al.

517 (2013) took place near the same location as the current study (i.e. the same military base), and the

518 ERs for HCN they report are not significantly different from the present measurements. This

519 suggests that the ratio of initial gases released of HCN to CO is consistent with the ratio of these

520 gases over the duration of the fire, or at least the fire-averaged ratio. With regards to ERs for HCN,

521 the major factor that appears to influence these values is fuel type, particularly the fuel's peat

522 content. Both laboratory (Stockwell et al., 2014) and field (Stockwell et al., 2016) studies of

523 Indonesian peat have shown greatly enhanced ERs for HCN compared to the studies represented

524   in Figure 7b, which consist mostly of pine, grasses and fuels of non-peat origin. The range in the

525   averages of ERs for HCN shown in Figure 7b is 0.0028–0.0095; the averages for the Indonesian

526   peat in laboratory and field studies were 0.015 and 0.021, respectively (Stockwell et al., 2014;

527   Stockwell et al., 2016), and interestingly are ~an order of magnitude greater than the range of

528   values seen in Figure 7b.
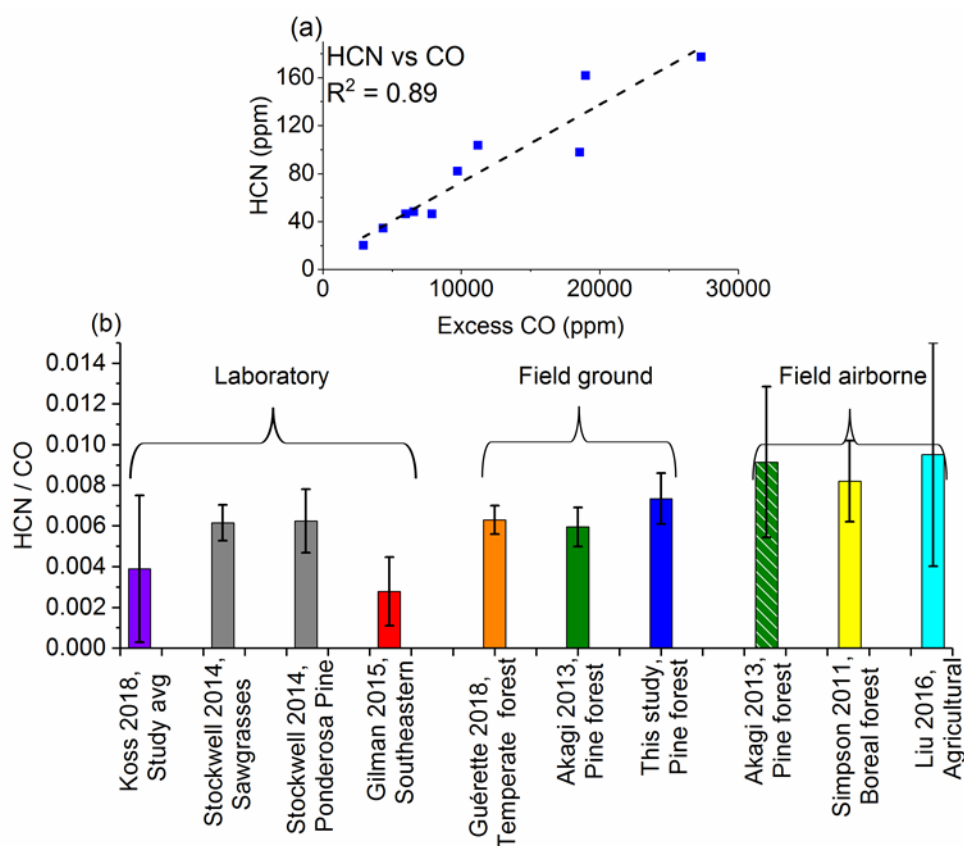
529
530   **Figure 7.** (a) Mixing ratios (ppm) for HCN as a function of excess CO (ppm) measured by FTIR. The dashed line is
531   a linear fit. (b) Average emission ratios (ppm_{HCN}/ppm_{CO}) for this study and previous laboratory and field
532   investigations. Error bars represent 1σ. Koss et al. (2018) and Stockwell et al. (2014) present fire-integrated ERs.
533   Gilman et al. (2015) present discrete ERs with sample acquisition of 20–300 s. Simpson et al. (2011) present fire-
534   averaged ERs derived by regression. Guérette et al. (2018) present a single ER from all fires and derived by regression.
535   Akagi et al. (2013) and Liu et al. (2016) present fire-averaged EFs calculated using ERs derived by regression. The
536   ERs for Akagi et al. (2013) and Liu et al (2016) were derived from the ratio of the EFs for HCN and CO multiplied
537   by the molar mass CO/molar mass HCN.

538

539   In the present study, trace amounts of HONO were detected, but NH_3 was not observed. The

540   absence of NH_3 was somewhat unexpected since, similar to HCN, it is a known product from the

541   pyrolysis of amino acids (Haidar et al., 1981) and has been observed in prior prescribed fires

542   conducted at Ft. Jackson (Akagi et al., 2014; Akagi et al., 2013). There are several possible

543   explanations for the lack of NH_3 in the measurements. First and foremost, experimentally NH_3 is

544   well known to adhere to certain surfaces (e.g. steel), and in this study it may have adhered to the

545   canisters or tubing walls and was thus not detected (Neuman et al., 1999; Roscioli et al., 2015;

546   Stockwell et al., 2014; Yokelson et al., 2003). Second, Sekimoto et al. (2018) observed that NH_3

547   is more often associated with a low temperature pyrolysis profile, and it appears that the present

548   samples were extracted during a period when high temperature pyrolysis was the main process.

549   Third, NH_3 is strongly linked with the smoldering phase (Goode et al., 1999; Yokelson et al.,

550   1996), and samples were not collected during this phase. Fourth, the speciation of the N-species

551   emitted is dependent on the fuel composition and amount of oxygen (Ren and Zhao, 2013b, a,

552   2012), so it is possible that in the present study the conditions favored HCN instead of NH_3.

553

554   The IR quantification of other N-species, such as NO, NO_2, CH_3NO_2 and HNCO was obstructed

555   due to interferences from H_2O, CO and CO_2 as well as the low emission values for some of these

556   N-species. Specifically, NO and NO_2 were likely not observed as these species are usually

557   associated with flaming combustion. HNCO has been linked with pyrolysis processes, and its main

558   formation pathway is the cracking of cyclic amides along with HCN which is also a product of

559   pyrolysis (Hansson et al. 2004). After accounting for the challenges in measuring NO, NO_2 and

560   HNCO, the second most prevalent N-containing species observed in this work was methyl nitrite

561   (CH_3ONO). Methyl nitrite has previously been detected in emissions from biomass burning using

562   other methods (Gilman et al., 2015). Figure 8a shows the plot of mixing ratios for methyl nitrite

563   as a function of excess CO. Unlike HCN (Figure 7a), methyl nitrite exhibits only minimal

564 correlation with excess CO. As one possible alternative explanation, methyl nitrite is known to be

565 associated with rocket-propelled grenades (RPGs), but the Ft. Jackson military base records did

566 not indicate RPG usage for these burn plots (Scharko et al., 2019). While few fire studies have

567 observed methyl nitrite, Gilman et al. (2015) have detected it using GC-MS. Figure 8b shows a

568 comparison of the results from Gilman et al. (2015), separated by U.S. region, with the present

569 results. It is worthy to note that both studies observed similar ERs and that in the Gilman study,

570 methyl nitrite had the second highest mean ER after HCN for N-bearing species in southwestern

571 fuels. Our observation of methyl nitrite is thus not unprecedented, but this was its first reported

572 detection via FTIR (Scharko et al., 2019) . In the present study, three measurements (Site 16, plot

573 1, msmt 1; Plot 24A, msmt 3; and Plot 24B) had higher ERs for methyl nitrite than the others, and

574 it is unclear why this is the case. Other measurements collected at the same location reported lower

575 ER values. If the three highest ER measurements in question are not included in the regression

576 then the correlation between methyl nitrite and CO is stronger, and the average ER is closer to

577 values reported by Gilman et al. (2015) for southeastern fuels. One possible explanation for the

578 three greater ER values is that the fuels may have contained more components such as nitrate esters

579 and isopropyl nitrate, both of which are known to release minor amounts of methyl nitrite under

580 controlled pyrolysis conditions (Boschan et al., 1955; Griffiths et al., 1975).
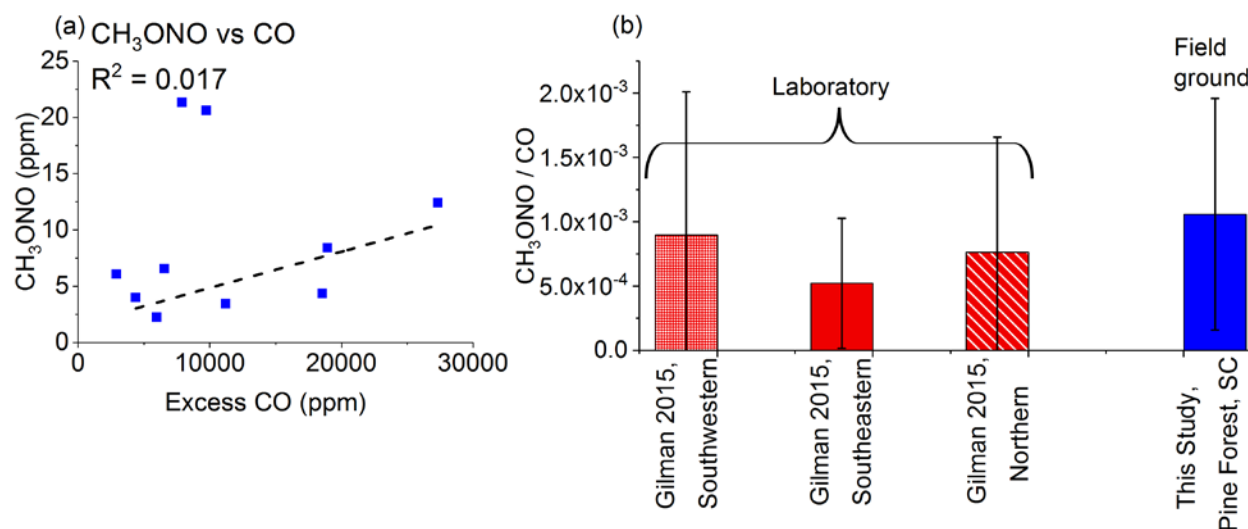
581
582 **Figure 8.** (a) Mixing ratios (ppm) for methyl nitrite (CH_3ONO) as a function of excess CO (ppm) as measured by
583 FTIR. The dashed line is a linear fit. (b) Average emission ratios (ppm_{CH3ONO}/ppm_{CO}) for this study and a previously
584 published study carried out in the laboratory using different fuels representative of three U.S. regions. Error bars
585 represent 1σ. Gilman et al. (2015) present discrete ERs with sample acquisition of 20 to 300 s.
586

4. CONCLUSIONS

587

588 While it is clearly important to sample fires as was done in this prescribed fire study, it is also

589 important to recall that significant differences may exist in the emissions between wildfire and

590 prescribed fire. As pointed out by Liu et al. (2017), there is far more particulate matter emitted

591 from a wildfire than for a controlled prescribed fire. Other differences in emissions from

592 prescribed fires and wildfires must surely exist, e.g. fuel consumption, fire meteorology, etc. This

593 paper only explores gas-phase emissions of the early stages of prescribe fires in the southeastern

594 U.S.

595 The main objective of this study was to collect and quantify gas-phase compounds emitted ahead

596 of the flame front (prior to the onset of combustion) in prescribed burns conducted in a pine forest.

597 Primary and secondary decomposition pathways generate volatile products, which in turn can act

598 as fuel gases that undergo combustion and contribute to sustaining the fire. The main observations

599 are that the estimated ratio of high-to-low temperature VOC emissions suggest that the samples

600 were indeed extracted when the high temperature pyrolysis process was dominant. The

601 acetylene/furan ratio suggested by Sekimoto et al. (2018) was nearly 10x higher than previous

602 studies; this is in fact consistent as previous works all had longer collection times, and in some

603 cases fire-averaged values. The significantly greater ERs observed for specific compounds, e.g.

604 lightweight HCs such as ethene and acetylene as well as unoxidized aromatics such as naphthalene

605 all support the hypothesis that the grab samples were collected prior to onset of decomposition,

606 recombination or combustion reactions, and that such gases represent pyrolytic processes. For the

607 oxidized organics, acetaldehyde and methanol consistently had the highest ER values relative to

608 CO for this collection of pyrolysis gases. The ERs for acetic acid and formaldehyde were found to

609 be high in some instances, but this appeared to be related to fuel composition of the individual

610 burn site. The major N-component released was HCN, while NH_3 was not observed. This is

611 consistent with the collected gases representing species associated with the high temperature

612 pyrolysis process, but the collection of NH_3 and amines in such systems is always problematic due

613 to wall adhesion. It would be interesting to study the effects of initial pyrolysis gas composition

614 ratios on the composition of the downwind plume (Johnson et al., 2006; Johnson et al., 2009).

615

616

617 **ASSOCIATED CONTENT**

618 **Author contribution**

619 NKS, TLM, and TJJ contributed to the writing of this manuscript. AMO and RGT set up laboratory

620 and recorded infrared data. NKS, AMO and CAB provided data processing and analysis. SPB,

621 ENL, JC, BMC and GMB aided in collection of field samples. JC provided thermal imaging and

622   videography. RDO and JRC contributed to fuel characterization. DRW and TJJ were the project

623   managers.

624   **ACKNOWLEDGMENT**

625   This work was supported by the Department of Defense's Strategic Environmental Research and

626   Development Program (SERDP), Project RC-2640 and we gratefully acknowledge our sponsor for

627   their support. PNNL is operated for the U.S. Department of Energy by the Battelle Memorial

628   Institute under contract DE-AC06-76RLO 1830. We gratefully thank David W. T. Griffith for his

629   valuable guidance and direction using the program MALT5 for spectral analysis. We are grateful

630   to John Maitland and colleagues at Fort Jackson for hosting the field campaign and carrying out

631   the burns. We thank Olivia Williams for help with spectral analysis using MALT5. In addition, we

632   are thankful to Professor Michael L. Myrick and his students at the University of South Carolina

633   for hosting us in their laboratory and for their helpful support setting up the instrument. This paper

634   is dedicated to Angela "Nicole" Chadwick Hawkins, Fort Jackson Wildlife Biologist. Nicole was

635   a champion for the use of prescribed fire and the conservation of all natural resources, especially

636   the red-cockaded woodpecker and longleaf pine ecosystem. She dedicated much of her

637   professional career to bird conservation as an exceptionally dedicated and talented biologist.

638   Nicole was a devoted mother of three.

5. REFERENCES

Akagi, S. K., Yokelson, R. J., Wiedinmyer, C., Alvarado, M. J., Reid, J. S., Karl, T., Crounse, J. D., and Wennberg, P. O.: Emission factors for open and domestic biomass burning for use in atmospheric models, Atmos. Chem. Phys., 11, 4039-4072, 2011.

Akagi, S. K., Yokelson, R. J., Burling, I. R., Meinardi, S., Simpson, I., Blake, D. R., McMeeking, G. R., Sullivan, A., Lee, T., Kreidenweis, S., Urbanski, S., Reardon, J., Griffith, D. W. T., Johnson, T. J., and Weise, D. R.: Measurements of reactive trace gases and variable O_3 formation rates in some South Carolina biomass burning plumes, Atmos. Chem. Phys., 13, 1141-1165, 2013.

Akagi, S. K., Burling, I. R., Mendoza, A., Johnson, T. J., Cameron, M., Griffith, D. W. T., Paton-Walsh, C., Weise, D. R., Reardon, J., and Yokelson, R. J.: Field measurements of trace gases emitted by prescribed fires in southeastern US pine forests using an open-path FTIR system, Atmos. Chem. Phys., 14, 199-215, 2014.

Albini, F. A.: Estimating wildfire behavior and effects, USDA Forest Service General Technical Report, INT-30, 1976.

Alves, C. A., Gonçalves, C., Pio, C. A., Mirante, F., Caseiro, A., Tarelho, L., Freitas, M. C., and Viegas, D. X.: Smoke emissions from biomass burning in a Mediterranean shrubland, Atmos. Environ., 44, 3024-3033, 2010.

Amini, E., Safdari, M.-S., DeYoung, J. T., Weise, D. R., and Fletcher, T. H.: Characterization of pyrolysis products from slow pyrolysis of live and dead vegetation native to the southern United States, Fuel, 235, 1475-1491, https://doi.org/10.1016/j.fuel.2018.08.112, 2019a.

Amini, E., Safdari, M.-S., Weise, D. R., and Fletcher, T. H.: Pyrolysis Kinetics of Live and Dead Wildland Vegetation from the Southern United States, Journal of Analytical and Applied Pyrolysis, 2019b.

Andreae, M. O., Browell, E. V., Garstang, M., Gregory, G. L., Harriss, R. C., Hill, G. F., Jacob, D. J., Pereira, M. C., Sachse, G. W., Setzer, A. W., Silva Dias, P. L., Talbot, R. W., Torres, A. L., and Wofsy, S. C.: Biomass-burning emissions and associated haze layers over Amazonia, J. Geophys. Res. Atmos., 93, 1509-1527, 1988.

Andreae, M. O.: Biomass burning: Its history, use, and distribution and its impact on environmental quality and global climate, in: Global Biomass Burning: Atmospheric, Climatic, and Biospheric Implications, edited by: Levine, J. S., MIT Press, Cambridge, Mass, 3-21, 1991.
Andreae, M. O., Anderson, B. E., Blake, D. R., Bradshaw, J. D., Collins, J. E., Gregory, G. L., Sachse, G. W., and Shipham, M. C.: Influence of plumes from biomass burning on atmospheric chemistry over the equatorial and tropical South Atlantic during CITE 3, J. Geophys. Res. Atmos., 99, 12793-12808, 1994.

Andreae, M. O., and Merlet, P.: Emission of trace gases and aerosols from biomass burning, Global Biogeochem. Cycles, 15, 955-966, 2001.

685
686 Azeez, A. M., Meier, D., and Odermatt, J.: Temperature dependence of fast pyrolysis volatile
687 products from European and African biomasses, J. Anal. Appl. Pyrolysis, 90, 81-92, 2011.
688 Bai, X., Johnston, P., Sadula, S., and Brown, R. C.: Role of levoglucosan physiochemistry in
689 cellulose pyrolysis, J. Anal. Appl. Pyrolysis, 99, 58-65, 2013.
690
691 Boschan, R., Merrow, R. T., and van Dolah, R. W.: The chemistry of nitrate esters, Chem. Rev.,
692 55, 485-510, 1955.
693
694 Burling, I., Yokelson, R. J., Akagi, S., Urbanski, S., Wold, C. E., Griffith, D. W., Johnson, T. J.,
695 Reardon, J., and Weise, D.: Airborne and ground-based measurements of the trace gases and
696 particles emitted by prescribed fires in the United States, Atmos. Chem. Phys. , 11, 12197-
697 12216, 2011.
698
699 Burling, I. R., Yokelson, R. J., Griffith, D. W. T., Johnson, T. J., Veres, P., Roberts, J. M.,
700 Warneke, C., Urbanski, S. P., Reardon, J., Weise, D. R., Hao, W. M., and de Gouw, J.:
701 Laboratory measurements of trace gas emissions from biomass burning of fuel types from the
702 southeastern and southwestern United States, Atmos. Chem. Phys., 10, 11115-11130, 2010.
703
704 Cary, A.: Some relations of fire to longleaf pine, J. For., 30, 594-601, 1932.
705
706 Chi, C., Horn, D., Reznik, R., Zanders, D., Opferkuch, R., Nyers, J., Pierovich, J., Lavdas, L.,
707 Mcmahon, C., and Nelson, R.: Source assessment: prescribed burning, state of the art, US
708 Environmental Protection Agency, EPA (US) Report EPA-600/2-79-019h, 1979.
709
710 Christian, T. J., Kleiss, B., Yokelson, R. J., Holzinger, R., Crutzen, P. J., Hao, W. M., Saharjo, B.
711 H., and Ward, D. E.: Comprehensive laboratory measurements of biomass-burning emissions: 1.
712 Emissions from Indonesian, African, and other fuels, J. Geophys. Res. Atmos., 108, 4719,
713 10.1029/2003JD003704, 2003.
714
715 Christian, T. J., Kleiss, B., Yokelson, R. J., Holzinger, R., Crutzen, P. J., Hao, W. M., Shirai, T.,
716 and Blake, D. R.: Comprehensive laboratory measurements of biomass-burning emissions: 2.
717 First intercomparison of open-path FTIR, PTR-MS, and GC-MS/FID/ECD, J. Geophys. Res.
718 Atmos., 109, 2004.
719
720 Clark, M. M., Fletcher, T. H., and Linn, R. R.: A sub-grid, mixture–fraction-based
721 thermodynamic equilibrium model for gas phase combustion in FIRETEC: development and
722 results, International Journal of Wildland Fire, 19, 202-212, 2010.
723
724 Coggon, M. M., Veres, P. R., Yuan, B., Koss, A., Warneke, C., Gilman, J. B., Lerner, B. M.,
725 Peischl, J., Aikin, K. C., Stockwell, C. E., Hatch, L. E., Ryerson, T. B., Roberts, J. M., Yokelson,
726 R. J., and de Gouw, J. A.: Emissions of nitrogen-containing organic compounds from the burning
727 of herbaceous and arboraceous biomass: Fuel composition dependence and the variability of
728 commonly used nitrile tracers, Geophys. Res. Lett., 43, 9903-9912, 2016.
729

730 Collard, F.-X., and Blin, J.: A review on pyrolysis of biomass constituents: Mechanisms and
731 composition of the products obtained from the conversion of cellulose, hemicelluloses and
732 lignin, Renew. Sustainable Energy Rev., 38, 594-608, 2014.

734 Crutzen, P. J., Heidt, L. E., Krasnec, J. P., Pollock, W. H., and Seiler, W.: Biomass burning as a
735 source of atmospheric gases CO, H2, N2O, NO, CH3Cl and COS, Nature, 282, 253, 1979.

737 Crutzen, P. J., and Andreae, M. O.: Biomass burning in the tropics: Impact on atmospheric
738 chemistry and biogeochemical cycles, Science, 250, 1669-1678, 1990.

740 DeGroot, W. F., Pan, W.-P., Rahman, M. D., and Richards, G. N.: First chemical events in
741 pyrolysis of wood, Journal of Analytical and Applied Pyrolysis, 13, 221-231, 1988.

743 Di Blasi, C.: Modeling and simulation of combustion processes of charring and non-charring
744 solid fuels, Prog. Energy Combust. Sci., 19, 71-104, 1993.

746 Di Blasi, C.: Modeling chemical and physical processes of wood and biomass pyrolysis, Prog.
747 Energy Combust. Sci., 34, 47-90, 2008.

749 Dlugokencky, E., and Tans, P.: NOAA/ESRL www.esrl.noaa.gov/gmd/ccgg/trends/.
750 Fagernäs, L., Kuoppala, E., and Simell, P.: Polycyclic aromatic hydrocarbons in birch wood slow
751 pyrolysis products, Energy Fuels, 26, 6960-6970, 2012.

753 Fairburn, J. A., Behie, L. A., and Svrcek, W. Y.: Ultrapyrolysis of n-hexadecane in a novel
754 micro-reactor, Fuel, 69, 1537-1545, 1990.

756 Ferguson, S. C., Dahale, A., Shotorban, B., Mahalingam, S., and Weise, D. R.: The role of
757 moisture on combustion of pyrolysis gases in wildland fires, Combustion Science and
758 Technology, 185, 435-453, 2013.

760 Fernandes, P. M., and Botelho, H. S.: A review of prescribed burning effectiveness in fire hazard
761 reduction, Int. J. Wildland Fire, 12, 117-128, 2003.

763 Gilman, J. B., Lerner, B. M., Kuster, W. C., Goldan, P. D., Warneke, C., Veres, P. R., Roberts, J.
764 M., de Gouw, J. A., Burling, I. R., and Yokelson, R. J.: Biomass burning emissions and potential
765 air quality impacts of volatile organic compounds and other trace gases from fuels common in
766 the US, Atmos. Chem. Phys., 15, 13915-13938, 2015.

768 Goode, J. G., Yokelson, R. J., Susott, R. A., and Ward, D. E.: Trace gas emissions from
769 laboratory biomass fires measured by open-path Fourier transform infrared spectroscopy: Fires
770 in grass and surface fuels, J. Geophys. Res. Atmos. , 104, 21237-21245, 1999.

772 Goode, J. G., Yokelson, R. J., Ward, D. E., Susott, R. A., Babbitt, R. E., Davies, M. A., and Hao,
773 W. M.: Measurements of excess O_3, CO_2, CO, CH_4, C_2H_4, C_2H_2, HCN, NO, NH_3, HCOOH,
774 CH_3COOH, HCHO, and CH_3OH in 1997 Alaskan biomass burning plumes by airborne Fourier
775 transform infrared spectroscopy (AFTIR), J. Geophys. Res. Atmos. , 105, 22147-22166, 2000.

776
777 Gordon, I. E., Rothman, L. S., Hill, C., Kochanov, R. V., Tan, Y., Bernath, P. F., Birk, M.,
778 Boudon, V., Campargue, A., Chance, K. V., Drouin, B. J., Flaud, J.-M., Gamache, R. R.,
779 Hodges, J. T., Jacquemart, D., Perevalov, V. I., Perrin, A., Shine, K. P., Smith, M.-A. H.,
780 Tennyson, J., Toon, G. C., Tran, H., Tyuterev, V. G., Barbe, A., Császár, A. G., Devi, V. M.,
781 Furtenbacher, T., Harrison, J. J., Hartmann, J.-M., Jolly, A., Johnson, T. J., Karman, T., Kleiner,
782 I., Kyuberis, A. A., Loos, J., Lyulin, O. M., Massie, S. T., Mikhailenko, S. N., Moazzen-Ahmadi,
783 N., Müller, H. S. P., Naumenko, O. V., Nikitin, A. V., Polyansky, O. L., Rey, M., Rotger, M.,
784 Sharpe, S. W., Sung, K., Starikova, D., Tashkun, S. A., Vander Auwera, J., Wagner, G.,
785 Wilzewski, J., Wcisło, P., Yu, S., and Zak, E. J.: The HITRAN2016 molecular spectroscopic
786 database, J. Quant. Spectrosc. Radiat. Transfer, 203, 3-69, 2017.
787
788 Griffith, D. W. T.: MALT5 User guide Version 5.5.9, 2016.
789
790 Griffiths, J. F., Gilligan, M. F., and Gray, P.: Pyrolysis of isopropyl nitrate. I. Decomposition at
791 low temperatures and pressures, Combust. Flame, 24, 11-19, 1975.
792
793 Guérette, E.-A., Paton-Walsh, C., Desservettaz, M., Smith, T. E., Volkova, L., Weston, C. J., and
794 Meyer, C. P.: Emissions of trace gases from Australian temperate forest fires: emission factors
795 and dependence on modified combustion efficiency, Atmos. Chem. Phys., 18, 3717-3735, 2018.
796 Haidar, N. F., Patterson, J. M., Moors, M., and Smith Jr, W. T.: Effects of structure on pyrolysis
797 gases from amino acids, J. Agric. Food Chem., 29, 163-165, 1981.
798
799 Hansson, K.-M., Samuelsson, J., Tullin, C., and Åmand, L.-E.: Formation of HNCO, HCN, and
800 NH_3 from the pyrolysis of bark and nitrogen-containing model compounds, Combust. Flame,
801 137, 265-277, 2004.
802
803 Hatch, L. E., Yokelson, R. J., Stockwell, C. E., Veres, P. R., Simpson, I. J., Blake, D. R.,
804 Orlando, J. J., and Barsanti, K. C.: Multi-instrument comparison and compilation of non-
805 methane organic gas emissions from biomass burning and implications for smoke-derived
806 secondary organic aerosol precursors, Atmos. Chem. Phys., 17, 1471-1489, 2017.
807
808 Hurst, D. F., Griffith, D. W. T., Carras, J. N., Williams, D. J., and Fraser, P. J.: Measurements of
809 trace gases emitted by Australian savanna fires during the 1990 dry season, J. Atmos. Chem., 18,
810 33-56, 1994a.
811
812 Hurst, D. F., Griffith, D. W. T., and Cook, G. D.: Trace gas emissions from biomass burning in
813 tropical Australian savannas, J. Geophys. Res. Atmos. , 99, 16441-16456, 1994b.
814
815 Johnson, T. J., Masiello, T., and Sharpe, S. W.: The quantitative infrared and NIR spectrum of
816 CH_2I_2 vapor: vibrational assignments and potential for atmospheric monitoring, Atmos. Chem.
817 Phys. , 6, 2581-2591, 2006.
818
819 Johnson, T. J., Sams, R. L., Burton, S. D., and Blake, T. A.: Absolute integrated intensities of
820 vapor-phase hydrogen peroxide (H_2O_2) in the mid-infrared at atmospheric pressure, Anal.
821 Bioanal. Chem., 395, 377-386, 2009.

822

823 Johnson, T. J., Profeta, L. T. M., Sams, R. L., Griffith, D. W. T., and Yokelson, R. L.: An
824 infrared spectral database for detection of gases emitted by biomass burning, Vib. Spectrosc., 53,
825 97-102, 2010.

826

827 Johnson, T. J., Sams, R. L., Profeta, L. T., Akagi, S. K., Burling, I. R., Yokelson, R. J., and
828 Williams, S. D.: Quantitative IR spectrum and vibrational assignments for glycolaldehyde vapor:
829 glycolaldehyde measurements in biomass burning plumes, J. Phys. Chem. A, 117, 4096-4107,
830 2013.

831

832 Johnson, W. R., and Kan, J. C.: Mechanisms of hydrogen cyanide formation from the pyrolysis
833 of amino acids and related compounds, J. Org. Chem., 36, 189-192, 1971.

834

835 Karl, T. G., Christian, T. J., Yokelson, R. J., Artaxo, P., Hao, W. M., and Guenther, A.: The
836 Tropical Forest and Fire Emissions Experiment: method evaluation of volatile organic compound
837 emissions measured by PTR-MS, FTIR, and GC from tropical biomass burning, Atmos. Chem.
838 Phys., 7, 5883-5897, 2007.

839

840 Kibet, J., Khachatryan, L., and Dellinger, B.: Molecular products and radicals from pyrolysis of
841 lignin, Environ. Sci. Technol., 46, 12994-13001, 2012.

842

843 Koss, A. R., Sekimoto, K., Gilman, J. B., Selimovic, V., Coggon, M. M., Zarzana, K. J., Yuan,
844 B., Lerner, B. M., Brown, S. S., Jimenez, J. L., Krechmer, J., Roberts, J. M., Warneke, C.,
845 Yokelson, R. J., and de Gouw, J.: Non-methane organic gas emissions from biomass burning:
846 identification, quantification, and emission factors from PTR-ToF during the FIREX 2016
847 laboratory experiment, Atmos. Chem. Phys., 18, 3299, 2018.

848

849 Ledesma, E. B., Marsh, N. D., Sandrowitz, A. K., and Wornat, M. J.: Global kinetic rate
850 parameters for the formation of polycyclic aromatic hydrocarbons from the pyrolyis of catechol,
851 a model compound representative of solid fuel moieties, Energy & fuels, 16, 1331-1336, 2002.

852

853 Lindenmaier, R., Tipton, N., Sams, R. L., Brauer, C. S., Blake, T. A., Williams, S. D., and
854 Johnson, T. J.: Assignment of the Fundamental Modes of Hydroxyacetone Using Gas-Phase
855 Infrared, Far-Infrared, Raman, and ab Initio Methods: Band Strengths for Atmospheric
856 Measurements, J. Phys. Chem. A, 120, 5993-6003, 2016.

857

858 Lindesay, J. A., Andreae, M. O., Goldammer, J. G., Harris, G., Annegarn, H. J., Garstang, M.,
859 Scholes, R. J., and Van Wilgen, B. W.: International geosphere-biosphere
860 programme/international global atmospheric chemistry SAFARI-92 field experiment:
861 Background and overview, J. Geophys. Res. Atmos., 101, 23521-23530, 1996.

862

863 Liu, X., Zhang, Y., Huey, L. G., Yokelson, R. J., Wang, Y., Jimenez, J. L., Campuzano-Jost, P.,
864 Beyersdorf, A. J., Blake, D. R., Choi, Y., St. Clair, H. M., Crounse, J. D., Day, D. A., Diskin, G.
865 S., Fried, A., Hall, S. R., Hanisco, T. F., King, L. E., Meinardi, S., Mikoviny, T., Palm, B. B.,
866 Peischl, J., Perring, A. E., Pollack, I. B., Ryerson, T. B., Sachse, G., Schwarz, J. P., Simpson, I.
867 J., Tanner, D. J., Thornhill, K. L., Ullmann, K., Weber, R. J., Wennberg, P. O., Wisthaler, A.,

Wolfe, G. M., and Ziemba, L. D.: Agricultural fires in the southeastern US during SEAC4RS: Emissions of trace gases and particles and evolution of ozone, reactive nitrogen, and organic aerosol, Journal of Geophysical Research: Atmospheres, 121, 7383-7414, https://doi.org/10.1002/2016JD025040, 2016.

Liu, X., Huey, L. G., Yokelson, R. J., Selimovic, V., Simpson, I. J., Müller, M., Jimenez, J. L., Campuzano-Jost, P., Beyersdorf, A. J., Blake, D. R., Butterfield, Z., Choi, Y., Crounse, J. D., Day, D. A., Diskin, G. S., Dubey, M. K., Fortner, E., Hanisco, T. F., Hu, W., King, L. E., Kleinman, L., Meinardi, S., Milkoviny, T., Onasch, T. B., Palm, B. B., Peischl, J., Pollack, I. B., Ryerson, T. B., Sachse, G. W., Sedlacek, A. J., Shilling, J. E., Springston, S., St. Clair, J. M., Tanner, D. J., Teng, A. P., Wennberg, P. O., Wisthaler, A., and Wolfe, G. M.: Airborne measurements of western US wildfire emissions: Comparison with prescribed burning and air quality implications, Journal of Geophysical Research: Atmospheres, 122, 6108-6129, 2017. Lobert, J. M., Scharffe, D. H., Weimin, H., Kuhlbusch, T. A., Seuwen, R., Warneck, P., and Crutzen, P. J.: Experimental evaluation of biomass burning emissions: Nitrogen and carbon containing compounds, in: Global Biomass Burning. Atmospheric, climatic, and biospheric implications, 1991.

Lu, Q., Yang, X.-c., Dong, C.-q., Zhang, Z.-f., Zhang, X.-m., and Zhu, X.-f.: Influence of pyrolysis temperature and time on the cellulose fast pyrolysis products: Analytical Py-GC/MS study, J. Anal. Appl. Pyrolysis, 92, 430-438, 2011.

Mell, W., Maranghides, A., McDermott, R., and Manzello, S. L.: Numerical simulation and experiments of burning douglas fir trees, Combustion and Flame, 156, 2023-2041, 2009. Melvin, M. A.: National prescribed fire use survey report, Coalition of Prescribed Fire Councils Technical Report, 01-12, 2012.

Miller, J. D., Safford, H. D., Crimmins, M., and Thode, A. E.: Quantitative evidence for increasing forest fire severity in the Sierra Nevada and southern Cascade Mountains, California and Nevada, USA, Ecosystems, 12, 16-32, 2009.

Neuman, J., Huey, L., Ryerson, T., and Fahey, D.: Study of inlet materials for sampling atmospheric nitric acid, Environmental Science & Technology, 33, 1133-1136, 1999.

Palma, C. F.: Modelling of tar formation and evolution for biomass gasification: a review, Appl. Energy, 111, 129-141, 2013.

Paton-Walsh, C., Wilson, S. R., Jones, N. B., and Griffith, D. W. T.: Measurement of methanol emissions from Australian wildfires by ground-based solar Fourier transform spectroscopy, Geophys. Res. Lett., 35, 2008.

Paton-Walsh, C., Deutscher, N. M., Griffith, D. W. T., Forgan, B. W., Wilson, S. R., Jones, N. B., and Edwards, D. P.: Trace gas emissions from savanna fires in northern Australia, J. Geophys. Res. Atmos., 115, 2010.

Porcher, R. D., and Rayner, D. A.: A guide to the wildflowers of South Carolina, University of South Carolina Press Columbia, South Carolina, 2001.

Prichard, S., Ottmar, R., and Anderson, G.: Consume 3.0 user's guide. USDA Forest Service, p. 234, 2006.

Reinhardt, E. D., Keane, R. E., and Brown, J. K.: First order fire effects model: FOFEM 4.0, user's guide, Gen. Tech. Rep. INT-GTR-344. Ogden, UT: US Department of Agriculture, Forest Service, Intermountain Research Station. 65 p., 344, 1997.

Ren, Q., and Zhao, C.: NO_x and N_2O precursors from biomass pyrolysis: Nitrogen transformation from amino acid, Environ. Sci. Technol., 46, 4236-4240, 2012.

Ren, Q., and Zhao, C.: NO_x and N_2O precursors from biomass pyrolysis: role of cellulose, hemicellulose and lignin, Environ. Sci. Technol., 47, 8955-8961, 2013a.

Ren, Q., and Zhao, C.: NO_x and N_2O precursors (NH_3 and HCN) from biomass pyrolysis: interaction between amino acid and mineral matter, Appl. Energy, 112, 170-174, 2013b.

Richter, H., and Howard, J. B.: Formation of polycyclic aromatic hydrocarbons and their growth to soot—a review of chemical reaction pathways, Prog. Energy Combust. Sci., 26, 565-608, 2000.

Roberts, J. M., Veres, P., Warneke, C., Neuman, J. A., Washenfelder, R. A., Brown, S. S., Baasandorj, M., Burkholder, J. B., Burling, I. R., and Johnson, T. J.: Measurement of HONO, HNCO, and other inorganic acids by negative-ion proton-transfer chemical-ionization mass spectrometry (NI-PT-CIMS): Application to biomass burning emissions, Atmos. Meas. Tech., 3, 981, 2010.

Roscioli, J., Zahniser, M., Nelson, D., Herndon, S., and Kolb, C.: New Approaches to measuring sticky molecules: improvement of instrumental response times using active passivation, The Journal of Physical Chemistry A, 120, 1347-1357, 2015.

Rothermel, R. C.: A mathematical model for predicting fire spread in wildland fuels, INT-115, 1972.

Safdari, M.-S., Rahmati, M., Amini, E., Howarth, J. E., Berryhill, J. P., Dietenberger, M., Weise, D. R., and Fletcher, T. H.: Characterization of pyrolysis products from fast pyrolysis of live and dead vegetation native to the Southern United States, Fuel, 229, 151-166, 2018.

Safdari, M.-S., Amini, E., Weise, D. R., and Fletcher, T. H.: Heating rate and temperature effects on pyrolysis products from live wildland fuels, Fuel, 242, 295-304, 2019.

Scharko, N. K., Oeck, A. M., Tonkyn, R. G., Baker, S. P., Lincoln, E. N., Chong, J., Corcoran, B. M., Burke, G. M., Weise, D. R., Myers, T. L., Banach, C. A., Griffith, D. W. T., and Johnson, T. J.: Identification of gas-phase pyrolysis products in a prescribed fire: first detections using

959   infrared spectroscopy for naphthalene, methyl nitrite, allene, acrolein and acetaldehyde, Atmos.
960   Meas. Tech., 12, 763-776, 10.5194/amt-12-763-2019, 2019.

962   Seinfeld, J. H., and Pandis, S. N.: Atmospheric chemistry and physics: from air pollution to
963   climate change, John Wiley & Sons, 2012.

965   Sekimoto, K., Koss, A. R., Gilman, J. B., Selimovic, V., Coggon, M. M., Zarzana, K. J., Yuan,
966   B., Lerner, B. M., Brown, S. S., Warneke, C., Yokelson, R. J., Roberts, J. M., and de Gouw, J.:
967   High-and low-temperature pyrolysis profiles describe volatile organic compound emissions from
968   western US wildfire fuels, Atmospheric Chemistry & Physics, 18, 2018.

970   Selimovic, V., Yokelson, R. J., Warneke, C., Roberts, J. M., Gouw, J. d., Reardon, J., and
971   Griffith, D. W. T.: Aerosol optical properties and trace gas emissions by PAX and OP-FTIR for
972   laboratory-simulated western US wildfires during FIREX, Atmos. Chem. Phys., 18, 2929-2948,
973   2018.

975   Shafizadeh, F., McGinnis, G., and Philpot, C.: Thermal degradation of xylan and related model
976   compounds, Carbohydr. Res., 25, 23-33, 1972.

978   Sharpe, S. W., Johnson, T. J., Sams, R. L., Chu, P. M., Rhoderick, G. C., and Johnson, P. A.:
979   Gas-phase databases for quantitative infrared spectroscopy, Appl. Spectrosc., 58, 1452-1461,
980   2004.

982   Shen, D., Gu, S., and Bridgwater, A. V.: Study on the pyrolytic behaviour of xylan-based
983   hemicellulose using TG–FTIR and Py–GC–FTIR, J. Anal. Appl. Pyrolysis, 87, 199-206, 2010.
984   Shen, D., Jin, W., Hu, J., Xiao, R., and Luo, K.: An overview on fast pyrolysis of the main
985   constituents in lignocellulosic biomass to valued-added chemicals: Structures, pathways and
986   interactions, Renew. Sustainable Energy Rev., 51, 761-774, 2015.

988   Shen, D. K., and Gu, S.: The mechanism for thermal decomposition of cellulose and its main
989   products, Bioresour. Technol., 100, 6496-6504, https://doi.org/10.1016/j.biortech.2009.06.095,
990   2009.

992   Shotorban, B., Yashwanth, B. L., Mahalingam, S., and Haring, D. J.: An investigation of
993   pyrolysis and ignition of moist leaf-like fuel subject to convective heating, Combustion and
994   flame, 190, 25-35, 2018.

996   Simmie, J. M.: Detailed chemical kinetic models for the combustion of hydrocarbon fuels, Prog.
997   Energy Combust. Sci., 29, 599-634, 2003.

999   Simpson, I. J., Akagi, S. K., Barletta, B., Blake, N. J., Choi, Y., Diskin, G. S., Fried, A.,
1000 Fuelberg, H. E., Meinardi, S., and Rowland, F. S.: Boreal forest fire emissions in fresh Canadian
1001 smoke plumes: C_1-C_{10} volatile organic compounds (VOCs), CO_2, CO, NO_2, NO, HCN and
1002 CH_3CN, Atmos. Chem. Phys., 11, 6445-6463, 2011.

Stein, Y. S., Antal Jr, M. J., and Jones jr, M.: A study of the gas-phase pyrolysis of glycerol, J. Anal. Appl. Pyrolysis, 4, 283-296, 1983.

Stockwell, C. E., Yokelson, R., Kreidenweis, S. M., Robinson, A. L., DeMott, P. J., Sullivan, R. C., Reardon, J., Ryan, K. C., Griffith, D. W. T., and Stevens, L.: Trace gas emissions from combustion of peat, crop residue, domestic biofuels, grasses, and other fuels: configuration and Fourier transform infrared (FTIR) component of the fourth Fire Lab at Missoula Experiment (FLAME-4), Atmos. Chem. Phys., 14, 9727-9754, 2014.

Stockwell, C. E., Jayarathne, T., Cochrane, M. A., Ryan, K. C., Putra, E. I., Saharjo, B. H., Nurhayati, A. D., Albar, I., Blake, D. R., Simpson, I. J., Stone, E. A., and Yokelson, R. J.: Field measurements of trace gases and aerosols emitted by peat fires in Central Kalimantan, Indonesia, during the 2015 El Niño, Atmos. Chem. Phys., 16, 11711-11732, 2016.

Talbot, R. W., Beecher, K. M., Harriss, R. C., and Cofer, W. R.: Atmospheric geochemistry of formic and acetic acids at a mid-latitude temperate site, J. Geophys. Res. Atmos., 93, 1638-1652, 1988.

Turetsky, M. R., Kane, E. S., Harden, J. W., Ottmar, R. D., Manies, K. L., Hoy, E., and Kasischke, E. S.: Recent acceleration of biomass burning and carbon losses in Alaskan forests and peatlands, Nat. Geosci., 4, 27, 2011.

Urbanski, S. P.: Combustion efficiency and emission factors for wildfire-season fires in mixed conifer forests of the northern Rocky Mountains, US, Atmos. Chem. Phys., 13, 7241-7262, 2013.
Waldrop, T. A., and Goodrick, S. L.: Introduction to prescribed fires in Southern ecosystems, Science Update SRS-054. Asheville, NC: US Department of Agriculture Forest Service, Southern Research Station. 80 p., 54, 1-80, 2012.

Ward, D., Susott, R., Kauffman, J., Babbitt, R., Cummings, D., Dias, B., Holben, B., Kaufman, Y., Rasmussen, R., and Setzer, A.: Smoke and fire characteristics for cerrado and deforestation burns in Brazil: BASE-B experiment, J. Geophys. Res. Atmos. , 97, 14601-14619, 1992.

Ward, D., and Radke, L.: Emissions measurements from vegetation fires: A comparative evaluation of methods and results, In: Crutzen, PJ; Goldammer, JG, eds. Fire in the Environment: The Ecological, Atmospheric, and Climatic Importance of Vegetation Fires. Dahlem Workshop Reports: Environmental Sciences Research Report 13. Chischester, England: John Wiley & Sons. p. 53-76., 1993.

Ward, D. E., and Hao, W.: Projections of emissions from burning of biomass for use in studies of global climate and atmospheric chemistry, Paper 91-128.4. Presented at the 84th Annual Meeting and Exhibition; Vancouver, British Columbia; June 16-21, 1991. Air and Waste Management Association. 16 p., 1991.

Ward, D. E., and Hardy, C. C.: Smoke emissions from wildland fires, Environ. Int., 17, 117-134, 1991.

1049 Ward, D. E., Hao, W. M., Susott, R. A., Babbitt, R. E., Shea, R. W., Kauffman, J. B., and Justice,
1050 C. O.: Effect of fuel composition on combustion efficiency and emission factors for African
1051 savanna ecosystems, J. Geophys. Res. Atmos., 101, 23569-23576, 1996.
1052
1053 Weise, D. R., Fletcher, T. H., Johnson, T. J., Hao, W., Dietenberger, M., Princevac, M., Butler,
1054 B., McAllister, S., O'Brien, J., Loudermilk, L., Ottmar, R. D., Hudak, A., Kato, A., Shotorban,
1055 B., Mahalingam, S., and Mell, W. E.: A project to measure and model pyrolysis to improve
1056 prediction of prescribed fire behavior [Chapter 3], In: Viegas, DX, ed. Advances in Forest Fire
1057 Research 2018. Coimbra, Portugal: Imprensa da Universidade de Coimbra. p. 308-218., 308-218,
1058 2018.
1059
1060 Wooster, M. J., Freeborn, P. H., Archibald, S., Oppenheimer, C., Roberts, G. J., Smith, T. E. L.,
1061 Govender, N., Burton, M., and Palumbo, I.: Field determination of biomass burning emission
1062 ratios and factors via open-path FTIR spectroscopy and fire radiative power assessment:
1063 headfire, backfire and residual smouldering combustion in African savannahs, Atmos. Chem.
1064 Phys., 11, 11591-11615, 2011.
1065
1066 Yashwanth, B., Shotorban, B., Mahalingam, S., Lautenberger, C., and Weise, D.: A numerical
1067 investigation of the influence of radiation and moisture content on pyrolysis and ignition of a
1068 leaf-like fuel element, Combustion and Flame, 163, 301-316, 2016.
1069
1070 Yokelson, R. J., Griffith, D. W. T., and Ward, D. E.: Open-path Fourier transform infrared
1071 studies of large-scale laboratory biomass fires, J. Geophys. Res. Atmos., 101, 21067-21080,
1072 1996.
1073
1074 Yokelson, R. J., Susott, R., Ward, D. E., Reardon, J., and Griffith, D. W. T.: Emissions from
1075 smoldering combustion of biomass measured by open-path Fourier transform infrared
1076 spectroscopy, J. Geophys. Res. Atmos., 102, 18865-18877, 1997.
1077
1078 Yokelson, R. J., Goode, J. G., Ward, D. E., Susott, R. A., Babbitt, R. E., Wade, D. D., Bertschi,
1079 I., Griffith, D. W. T., and Hao, W. M.: Emissions of formaldehyde, acetic acid, methanol, and
1080 other trace gases from biomass fires in North Carolina measured by airborne Fourier transform
1081 infrared spectroscopy, J. Geophys. Res. Atmos., 104, 30109-30125, 1999.
1082
1083 Yokelson, R. J., Christian, T. J., Bertschi, I. T., and Hao, W. M.: Evaluation of adsorption effects
1084 on measurements of ammonia, acetic acid, and methanol, Journal of Geophysical Research:
1085 Atmospheres, 108, 2003.
1086
1087 Yokelson, R. J., Crounse, J. D., DeCarlo, P. F., Karl, T., Urbanski, S. P., Atlas, E., Campos, T.,
1088 Shinozuka, Y., Kasputin, V., Clarke, A. D., Weinheimer, A., Knapp, D. J., Montzka, D. D.,
1089 Holloway, J., Weibring, P., Flocke, F., Zheng, W., Toohey, D., Wennberg, P. O., Wiedinmyer,
1090 C., Mauldin, L., Fried, A., Richter, D., Walega, J., Jimenez, J. L., Adachi, K., Buseck, P. R.,
1091 Hall, S. R., and Shetter, R.: Emissions from biomass burning in the Yucatan, Atmos. Chem.
1092 Phys., 9, 5785, 2009.
1093

1094   Yokelson, R. J., Burling, I. R., Gilman, J. B., Warneke, C., Stockwell, C. E., Gouw, J. d., Akagi,
1095   S. K., Urbanski, S. P., Veres, P., Roberts, J. M., Kuster, W. C., Reardon, J., Griffith, D. W. T.,
1096   Johnson, T. J., Hosseini, S., Miller, J. W., Cocker III, D. R., Jung, H., and Weise, D. R.:
1097   Coupling field and laboratory measurements to estimate the emission factors of identified and
1098   unidentified trace gases for prescribed fires, Atmos. Chem. Phys., 13, 89-116, 2013.
1099
1100   Young, V. L., Kieser, B. N., Chen, S. P., and Niki, H.: Seasonal trends and local influences on
1101   nonmethane hydrocarbon concentrations in the Canadian boreal forest, J. Geophys. Res. Atmos.,
1102   102, 5913-5918, 1997.

1103